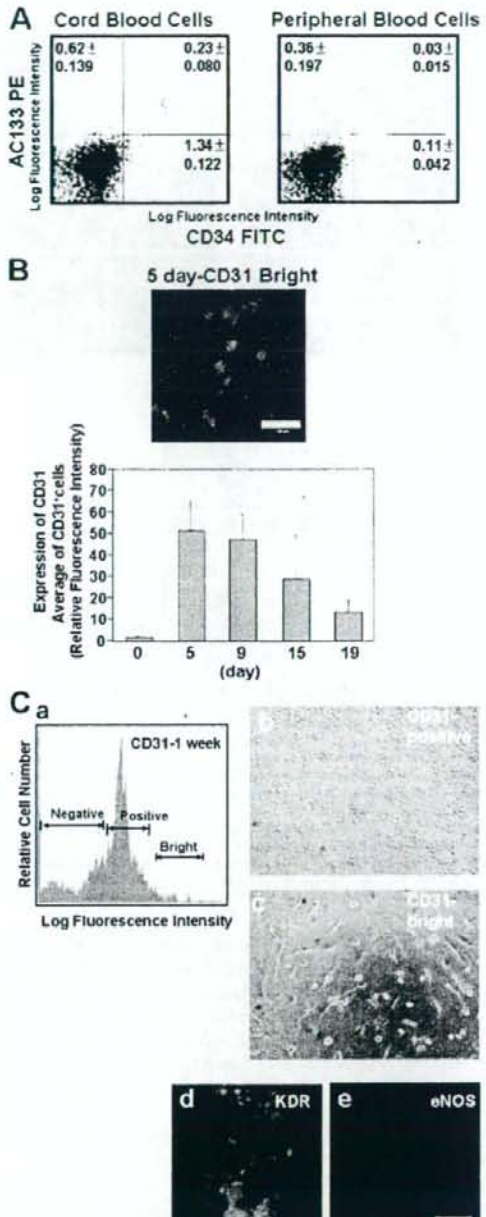

FIGURE 1. ***In vitro* differentiation of AC133$^+$ cells of cord blood into endothelial cells.** *A*, expression of AC133 and CD34 cells in human cord blood and peripheral blood mononuclear cells was analyzed by staining with AC133-PE (*vertical axis*) and CD34-FITC (*horizontal axis*). The *numbers* in the flow cytometric dot blots indicates the percentage of each population ± S.D. *B*, when AC133$^+$ cells were cultured for 19 days in the presence of VEGF on FN-coated dishes, the appearance of CD31$^+$ cells was analyzed. The *upper panel* shows the fluorescent photomicrograph of adhesion cells stained with FITC-conjugated anti-CD31 antibody after a 5-day culture. Quantitation of the fluorescence intensity of 20 CD31-positive cells was analyzed as described under "Experimental Procedures." Columns and bars represent the means ± S.D. from 20 cells (*B*, *lower panel*). *C*, the CD31-negative, positive, and bright cell populations prepared after 1-week cultivation of AC133$^+$ cells are shown in a representative histogram stained with FITC-conjugated anti-CD31 antibody. The *x* axis represents the log fluorescence intensity of CD31-FITC, *y* axis relative cell number (*panel a*). *Panels b* and *c* show phase-contrast microscopic photographs of cultured CD31-positive and bright cells, respectively, subsequently cultured for 1 week after cell sorting. The *bottom panels d* and *e* show the fluorescent photomicrographs of adhesion cells from the CD31^{bright} fraction stained with anti-KDR antibody and anti-eNOS antibody, respectively. *Scale bar*, 100 μm.

7.5), 1 mM EDTA, 5 mM EGTA, 10 mM $MgCl_2$, and 50 mM β-glycerophosphate, along with 1/100 (v/v) protease inhibitor mixture (Sigma) and 1/100 (v/v) phosphatase inhibitor mixture (Sigma). The cellular lysate of 5×10^5 cells/lane was subjected to Western blotting analysis.

Statistical Analysis—Statistical analysis was performed using the unpaired Student's *t* test, and the dose response of TPO was compared between the four groups by one-way analysis of variance and the Tukey test using Prism 4 software. Values of $p < 0.05$ were considered to indicate statistical significance. Each experiment was repeated three times, and the representative data are indicated.

RESULTS

We previously reported that during the *in vitro* differentiation of peripheral blood AC133$^+$ cells into the endothelial cells, the expression of CD31 was the earliest marker among all of the tested markers (25). Moreover, by analyzing the ability of differentiation into endothelial cells, CD31^{bright} cells were shown to exhibit EPC character when compared with the CD31$^+$ fraction. Since cord blood is a rich source of blood stem cells such as CD34$^+$ and AC133$^+$ cells, it is expected to be a useful source for CD31^{bright} cells. At first, we attempted to determine whether the CD31^{bright} fraction derived from cord blood AC133$^+$ cells contained EPCs. As shown in Fig. 1*A*, the populations of AC133$^+$ CD34$^-$ cells, AC133$^-$ CD34$^+$ cells, and AC133$^+$ CD34$^+$ cells in cord blood were approximately four times greater than those in peripheral blood (Fig. 1*A*). After 5 days of cultivation of AC133$^+$ cells on an FN-coated dish, adherent CD31-positive cells were observed (Fig. 1*B*, *upper panel*). Analysis of the fluorescence intensity of CD31-positive cells revealed that the average fluorescence intensity in CD31$^+$ cells was highest on day 5 (Fig. 1*B*, *lower panel*), corresponding to the results of peripheral blood cells.

After 1 week of cultivation of AC133$^+$ cells on a collagen type IV-coated dish, on which cells adhered more loosely when compared with the FN-coated dish, cells were collected and sorted into CD31$^+$ and CD31^{bright} fractions, as shown in Fig. 1*C*, *panel a*, and both cell types were cultured on an FN-coated dish for 1 week after the sorting. The number of cells adhering and spreading was higher in the CD31^{bright} fraction (Fig. 1*C*, *panel c*) than in the CD31$^+$ fraction (Fig. 1*C*, *panel b*), and these adhering cells are apparently KDR- (Fig. 1*C*, *panel d*) and eNOS-positive (Fig. 1*C*, *panel e*). The large areas of intense green fluorescence represent the colonies of CD31^{bright} cells. These data indicate that CD31^{bright} cells derived from AC133$^+$ cells of both peripheral blood and cord blood are EPCs.

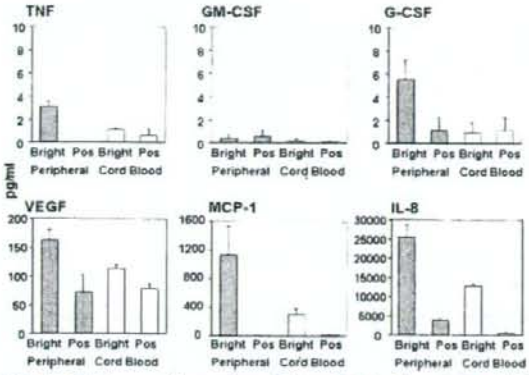

FIGURE 2. **Various cytokines released from CD31$^+$ cells and CD31^{bright} cells.** Production of various cytokines from CD31$^+$ cells and CD31^{bright} cells derived from AC133$^+$ cells cultivated for 5 days was measured. *Gray columns* indicate the cytokine production by cells from peripheral blood and open columns from cord blood. Columns and bars represent the means ± S.D. from three separate experiments. *TNF*, tumor necrosis factor; *Pos*, positive; *MCP-1*, monocyte chemoattractant protein-1.

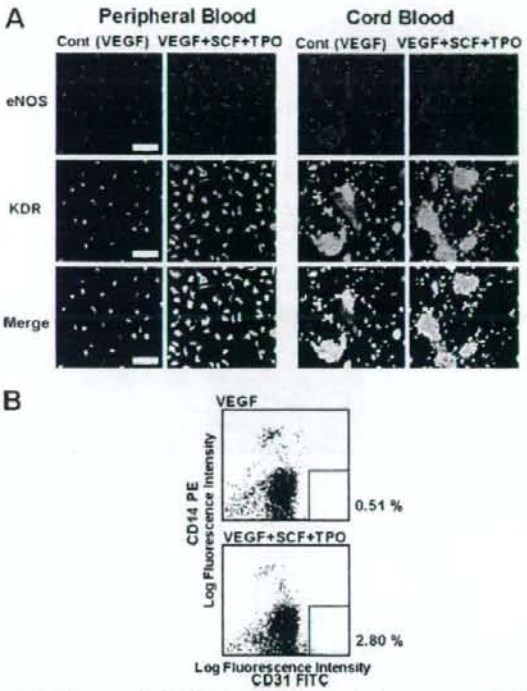

FIGURE 3. **Increment of EPCs from AC133$^+$ cells in the presence of TPO and SCF.** *A*, AC133$^+$ cells were differentiated for 2 weeks in the presence of either VEGF alone or the combination of TPO, SCF, and VEGF on an FN-coated dish. The *upper* and *middle panels* indicate the fluorescent photomicrographs of cells stained with anti-eNOS antibody and anti-KDR antibody, respectively. The *bottom panels* indicate the merged images of both antibodies. From the *left side*, control (*Cont*) and the mixture of peripheral blood, control, and the mixture of cord blood. *Scale bar*, 100 μm. *B*, CD14 and CD31 expression in cultured AC133$^+$ cells for 1 week was stained with CD14-PE (*vertical axis*) and CD31-FITC (*horizontal axis*). The *upper panel* indicates cells treated with VEGF alone, and the *lower panel* indicates cells treated with the mixture of VEGF, SCF, and TPO. The *number* on the *right side* of the flow cytometric dot blot indicates the percentage of the CD14$^-$ CD31^{bright} population.

Several reports have shown that EPCs produce cytokines (9, 26, 27), but the ability of CD31$^+$ or CD31^{bright} cells derived from AC133$^+$ cells to produce cytokines is not known. After cell sorting, quantitative analysis of cytokines released by CD31$^+$ cells and CD31^{bright} cells was carried out at 5 days after the cultivation. As shown in Fig. 2, IL-8 was markedly produced by CD31^{bright} cells from both peripheral blood and cord blood when compared with CD31$^+$ cells. The production of monocyte chemoattractant protein-1 (MCP-1) by CD31^{bright} cells was also higher than that of CD31$^+$ cells. The production of VEGF was higher by CD31^{bright} cells than by CD31$^+$ cells but not significantly. The production of all cytokines by CD31^{bright} cells from peripheral blood was higher than that from cord blood. Tumor necrosis factor-α, GM-CSF, and G-CSF were hardly produced by CD31^{bright} and CD31$^+$ cells. These data indicate that CD31^{bright} cells derived from AC133$^+$ cells have a strong ability to produce chemokines.

It has been reported that TPO and SCF are potent stimulators of multipotent cell proliferation (17, 19). Next, the effects of both growth factors on EPC growth and differentiation in our culture system were determined. After the addition of both TPO and SCF for 2 weeks, the expression of eNOS and KDR in adhered cells was analyzed (Fig. 3*A*). Fig. 3*A* clearly indicates that AC133$^+$ cells from both peripheral blood and cord blood differentiate into eNOS$^+$ and KDR$^+$ cells more efficiently in the presence of the mixture of TPO, SCF, and VEGF than of VEGF alone. Flow cytometric analysis revealed that the ratio of CD31^{bright} CD14$^-$ cells increased in the presence of the mixture of TPO, SCF, and VEGF when AC133$^+$ cells were cultured on collagen type IV-coated dish for 1 week (Fig. 3*B*).

We next examined which growth factor is dominant in the induction and proliferation of CD31^{bright} cells. The total cell number of cultured AC133$^+$ cells from both peripheral blood (Fig. 4*A*, *upper panel*) and cord blood (Fig. 4*A*, *lower panel*) significantly increased in the presence of TPO, SCF, or both growth factors when compared with that of VEGF alone during a 1-week period. As shown in Fig. 4*B*, however, the increment in the ratio of the CD31^{bright} cell population was observed only in the presence of TPO. The absolute number of CD31^{bright} cells, calculated by the total cell number and the ratio of the CD31^{bright} cell population, was markedly increased by TPO (Fig. 4*C*). In contrast, SCF induced the increase in total cell number to the same level as TPO (Fig. 4*A*), but it did not induce the increase in either the ratio of the CD31^{bright} cell population (Fig. 4*B*) or the number of CD31^{bright} cells (Fig. 4*C*). Next, we examined whether TPO and VEGF can synergistically affect the induction of CD31^{bright} cells during a 1-week cultivation. As shown in Fig. 4*D*, although VEGF had no effects on the total cell number (Fig. 4*D*, *panel a*), it increased the ratio of the CD31^{bright} cell population to 1.4-fold higher than that of the control (Fig. 4*D*, *panel b*), resulting in a slight increase in the number of CD31^{bright} cells (Fig. 4*D*, *panel c*). Thrombopoietin alone induced an increase in not only the total cell number (Fig. 4*D*, *panel a*) but also the ratio of the CD31^{bright} cell population (Fig. 4*D*, *panel b*), resulting in an ~24-fold increment of the absolute

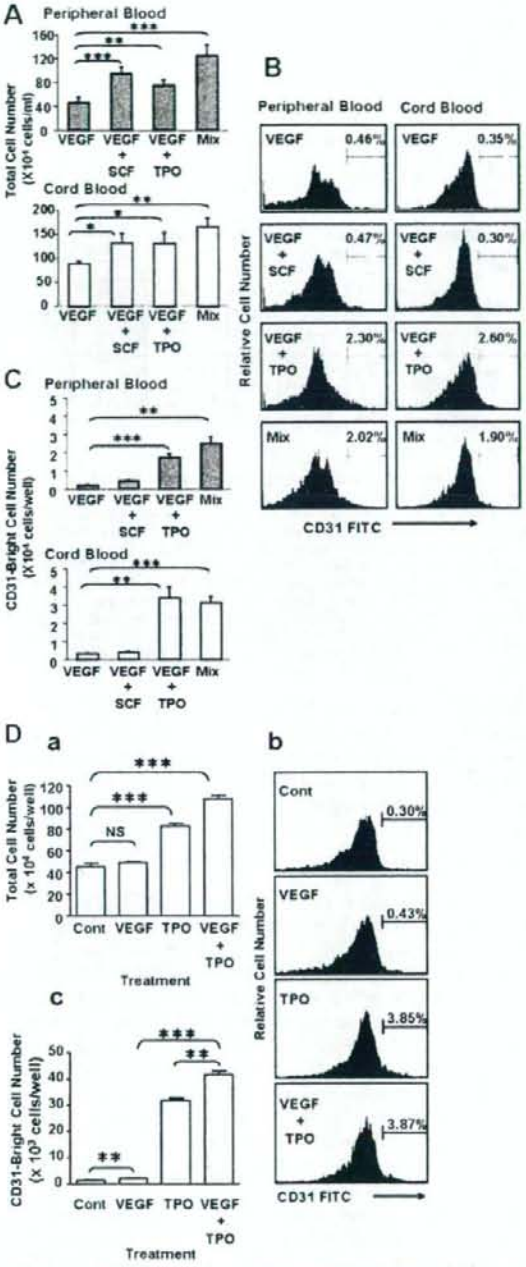

FIGURE 4. **Stimulative effects of TPO on induction of CD31^{bright} cells.** *A*, alteration of the cell number of cultivated AC133^{+} cells for 1 week in the combination of growth factors. *Mix*, VEGF + SCF + TPO. *B*, the flow cytometric histogram of AC133^{+}-derived cells stained with FITC-labeled anti-CD31 antibody after a 1-week culture. The *representing number* in the flow cytometric histogram indicates the percentage of the CD31^{bright} cell population. The *left panels* are peripheral blood, and the *right panels* are cord blood. *C*, CD31^{bright} cells numbers were calculated by both the total cell number and the ratio the of CD31^{bright} population. *D*, the effects of TPO alone on EPC differentiation derived from AC133^{+} cells of cord blood. The *upper left panel* (*a*) shows the total cell number after a 1-week culture, the *right panels* (*b*) show the flow cytometric histogram of AC133^{+}-derived cells stained with FITC-labeled anti-CD31 antibody, and the *lower left panel* (*c*) shows the calculated CD31^{bright} cell number. Columns and bars represent the means ± S.D. (*, $p < 0.05$; **, $p < 0.01$; ***, $p < 0.001$). *NS*, not significant; *Cont*, control.

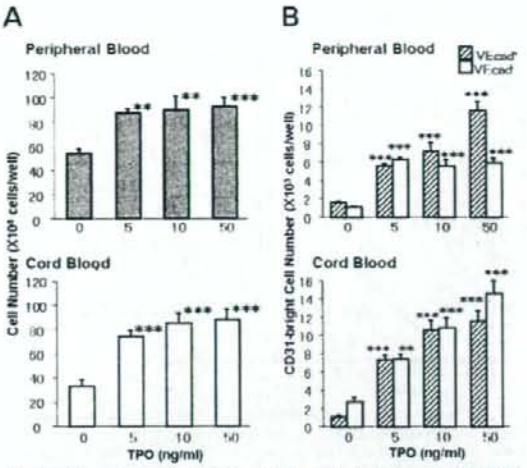

FIGURE 5. **Dose-dependent effects of TPO on the induction of CD31^{bright} cells from AC133^{+} cells.** AC133^{+} cells were treated with various concentrations of TPO for 1 week. The *left panels* (*A*) are the total cell number of cultured AC133^{+} cells from peripheral blood (*upper panel*) and cord blood (*lower panel*). The *right panels* (*B*) are the calculated CD31^{bright} cell number from peripheral blood (*upper panel*) and cord blood (*lower panel*). Columns and bars represent the means ± S.D. (**, $p < 0.01$; ***, $p < 0.001$). *Striped* and *dotted columns* represent CD31^{bright}VEcad^{-} cells and CD31^{bright}VEcad^{-} cells, respectively.

number of CD31^{bright} cells when compared with the control (Fig. 4*D*, *panel c*). The concomitant treatment with both VEGF and TPO showed a synergic increase in the number of CD31^{bright} cells (Fig. 4*D*, *panel c*).

When AC133^{+} cells were cultured with various concentrations of TPO in the presence of constant concentrations of VEGF (50 ng/ml), the total cell number from both peripheral blood (Fig. 5*A*, *upper panel*) and cord blood (Fig. 5*A*, *lower panel*) significantly increased at 5 ng/ml of TPO when compared with the control, and there was no significant difference in the total cell number from 5 to 50 ng/ml of TPO. However, TPO increased the ratio of CD31^{bright} cells of flow cytometry dose-dependently as follows: control, 0.50%; 5 ng/ml, 1.36%; 10 ng, 1.42%; 50 ng/ml 1.90% in peripheral blood and control, 1.16%; 5 ng/ml, 1.99%; 10 ng, 2.51%; 50 ng/ml 2.96% in cord blood. TPO markedly induced the differentiation of AC133^{+} cells into CD31^{bright}VEcad^{+} cells in the case of both peripheral blood (Fig. 5*B*, *upper panel*) and cord blood (Fig. 5*B*, *lower panel*) in a dose-dependent manner. In the case of cord blood cells, differentiation into CD31^{bright}VEcad^{-} cells was also induced by TPO.

The effects of TPO on total cell number during 6-day culture of AC133^{+} cells were determined. Although the total cell num-

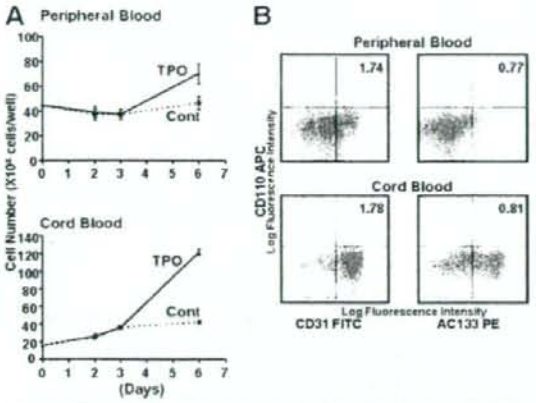

FIGURE 6. **Time-course analysis of TPO-treated AC133$^+$ cells and expression of TPO receptor (CD110).** *A*, alteration of cell number was counted at 2, 3, and 6 days. *Solid* and *dotted lines* indicate TPO-treated cells and control ((*Cont*) VEGF alone) cells, respectively. The results represent mean ± S.E. of triplicate wells. *B*, flow cytometric analysis of CD110 expression on AC133$^+$ cells cultured for 3 days was carried out. The *y axis* represents the log fluorescence intensity of CD110-allophycocyanin (*APC*), and the *x axis* represents that of CD31-FITC (*left panels*) and AC133-PE (*right panels*). The *number* in the flow cytometric dot blot indicates the percentage of CD110$^+$ CD31$^+$ and CD110$^+$ AC133$^+$ populations, respectively. The *upper panels* are peripheral blood, and the *lower panels* are cord blood.

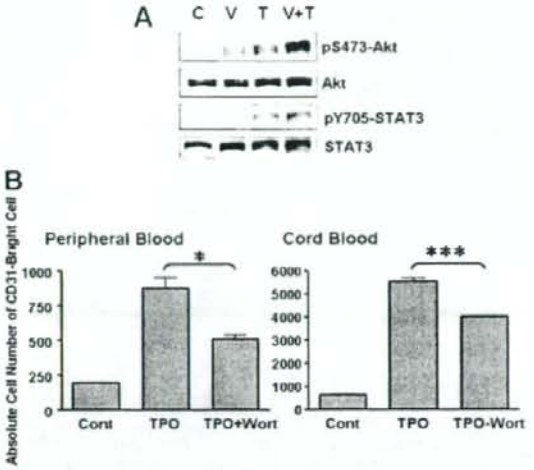

FIGURE 7. **Analysis of TPO-induced signal transduction on AC133$^+$ cells of cord blood.** *A*, activation of Akt or STAT3 was analyzed by Western blotting with anti-phospho-specific Ser-473-Akt antibody (*top panel*) and reprobed with anti-Akt antibody (*second panel*), or with anti-phospho-specific Tyr-705-STAT3 antibody (*third panel*) and reprobed with anti-STAT3 antibody (*lower panel*) after stimulation by VEGF, TPO, or both VEGF and TPO for 15 min using 3-day-cultured AC133$^+$ cells. *C*, control; *V*, VEGF; *T*, TPO. *B*, the effects of wortmannin on CD31^{bright} cell induction were investigated. The *right panel* shows peripheral blood, and the *left panel* shows cord blood. The *y axis* represents the CD31^{bright} cell number. *Wort*, 100 nM wortmannin. Columns and bars represent the means ± S.E. (*, $p < 0.05$; ***, $p < 0.001$). *Cont*, control.

ber from AC133$^+$ cells slightly and constantly increased from day 0 to day 6 in the absence of TPO, total cells markedly increased after the third day in the presence of TPO (Fig. 6*A*). Next, the alternation of TPO receptor (CD110) expression was analyzed during the cultivation of AC133$^+$ cells. Although the percentages of both AC133$^+$ CD110$^+$ cells and CD31$^+$ CD110$^+$ cells were 0% just after magnetic cell sorting, 3 days after the cultivation, ~2% of CD31$^+$ CD110$^+$ cells (Fig. 6*B*, *left panel*) and 1% of AC133$^+$ CD110$^+$ cells (Fig. 6*B*, *right panel*) appeared from AC133$^+$ cells in the peripheral blood and cord blood, respectively. These data indicate the possibility that sorted AC133$^+$ cells may differentiate into AC133$^+$ CD110$^+$ cells and may subsequently proliferate and differentiate into EPCs in response to TPO.

It has been reported that TPO activates the PI3K/Akt pathway (28) or JAK/STAT pathway (20, 29, 30) in target cells. In addition, in the present study, TPO induced a marked proliferation of AC133$^+$ cells after 3-day culture, and CD110 expression in cells cultured for 3 days from both cord blood and peripheral blood was also observed (Fig. 6, *A* and *B*). We then attempted to determine whether TPO activates Akt or STAT in AC133$^+$ cells cultured for 3 days by analyzing the phosphorylation at Ser-473 of Akt or the phosphorylation at Tyr-705 of STAT3, which are the active forms of Akt or STAT3, respectively. As shown in Fig. 7*A*, phosphorylation at Ser-473 of Akt was stimulated by both VEGF and TPO at 15 min and was more markedly stimulated by concomitant treatment with VEGF and TPO than by a single treatment (Fig. 7*A*, *top panel*). Phosphorylation at Tyr-705 of STAT3 was observed only in the presence of TPO, and unlike in the phosphorylation at Ser-473 of Akt, an increased amount of phosphorylation was not observed in the concomitant presence of VEGF and TPO (Fig. 7*A*, *third panel*). On the other hand, there was no difference in the expression of Akt and STAT3 protein levels (Fig. 7*A*, *second panel* and *bottom panel*, respectively). The induction of CD31^{bright} cells was not perfectly but significantly inhibited by wortmannin, an inhibitor of PI3K, suggesting that the PI3K/Akt pathway plays an important role in TPO-induced EPC differentiation (Fig. 7*B*).

DISCUSSION

We have previously reported that CD31^{bright} cells derived from AC133$^+$ cells in human peripheral blood are EPCs (25). In the present study, CD31^{bright} cells also appeared from AC133$^+$ cells prepared from cord blood, which are a rich source of stem cells during the early period of cultivation (Fig. 1, *A* and *B*). When cells were separated in terms of CD31 expression (Fig. 1*C*), CD31^{bright} cells differentiated into KDR-positive and eNOS-positive adherent cells. These data indicate that CD31^{bright} cells derived from AC133$^+$ cells in cord blood have some characteristics similar to those of EPCs in peripheral blood. Although these EPCs in both cord blood and peripheral blood could not form tube-like structure by themselves on Matrigel (data not shown), they secreted angiogenic growth factors (Fig. 2) such as VEGF, IL-8 (31, 32), and monocyte chemoattractant protein-1 (MCP-1) (33). It has been reported that there are at least two types of EPCs: early EPCs and late EPCs. Early EPCs are unable to form tube-like structures and secrete VEGF and IL-8 showing peak growth at 2–3 weeks (9, 26, 27). Late EPCs with the ability to proliferate and having a cobblestone shape appear late at 2–3 weeks, show exponential growth at 4–8 weeks, and have the ability to form tube-like structures

(26, 27, 34). Rehman *et al.* (9) have reported that EPCs derived from monocytes/macrophages do not proliferate but instead release potent proangiogenic growth factors. In many studies (9, 26, 27, 35–37), because the origin of early EPCs was $CD14^+$ cells or was not precluded by monocytic cells, CD14 expression was still observed in the EPCs after cultivation. In our study, in which $AC133^+$ cells were used as the origin of the EPCs, CD14 expression was not observed in $CD31^{bright}$ cells induced by TPO (Fig. 3*B*). Although the $CD31^{bright}$ cells identified as EPCs in this report and in a previous report did not correspond to their cells in terms of the origin of the cells or cell surface markers, these cells may be early EPCs that can release potent proangiogenic growth factors (Fig. 2). In any event, EPCs are thought to be a heterogeneous population, unlike late EPCs, which have a high ability to proliferate.

Circulating EPCs are up-regulated under physiological or pathological conditions and also by 3-hydroxy-3-methyl-glutaryl-CoA reductase inhibitors (14, 15) and cytokines such as erythropoietin (11–13) and G-CSF (10). In this report, we have revealed the possibility of marked expansion of EPCs *in vitro* by TPO. Brizzi *et al.* (20) have reported that TPO directly stimulates endothelial cell motility and neoangiogenesis. In the present study, TPO may have played a stimulatory role in the differentiation of EPCs from circulating stem cells.

Although both TPO and SCF have the same potency with regard to proliferation of $AC133^+$ cells (Fig. 4*A*), TPO specifically induces an increase in the ratio of the $CD31^{bright}$ cell population when compared with SCF (Fig. 4, *B* and *C*). To develop useful cell therapy products for severe ischemia, it has been considered desirable to establish the efficient expansion of EPCs *in vitro*. Thrombopoietin could increase $CD31^{bright}$ cells (EPCs) even in the absence of VEGF. Kirito *et al.* (38) have reported that TPO enhances expression of VEGF in hematopoietic cells through induction of hypoxia-inducible factor 1α. These observations suggest the possibility that the production of EPCs by TPO may be supported by VEGF produced by $AC133^+$ cells. However, from the perspective that TPO and VEGF have synergistic effects on the induction of EPCs, TPO seems to induce EPCs through another signaling cascade.

Thrombopoietin is a major regulator of the proliferation, differentiation, and maturation of megakaryocytes (39, 40). The results from recent studies suggest that TPO can act not only as a lineage-specific hematopoietic growth factor but also can affect other hematopoietic cell types. For example, TPO alone does not induce proliferation of long term repopulating hematopoietic stem cells. However, in combination with SCF or IL-3, TPO has several synergistic effects on cell proliferation (19). Our results have revealed a new role of TPO in the production of EPCs.

In the process of differentiation of $AC133^+$ cells into $CD31^{bright}$ cells, both peripheral blood and cord blood appear to be very similar. $AC133^+$ cells of cord blood, however, have a stronger ability to proliferate than those of peripheral blood (Fig. 6*A*). Moreover, TPO stimulates the induction of $CD31^{bright}VEcad^-$ cells only from cord blood (Fig. 5*B*) at high concentrations. Hur *et al.* (26) have reported that $VEcad^-$ EPCs are thought to be an early EPC. It is therefore thought that $AC133^+$ cells of cord blood are more immature than those of peripheral blood.

Although the total cell number treated with TPO slightly increased in a dose-dependent manner (Fig. 5*A*), the $CD31^{bright}$ cell number markedly increased as the TPO concentration increased (Fig. 5*B*). These data suggest the possibility that a higher concentration of TPO may be needed for $CD31^{bright}$ cell induction from $AC133^+$ cells.

When $AC133^+$ cells were stimulated by TPO or VEGF, an increase in the phosphorylation of Akt at Ser-473 was observed. This increase was strongly enhanced by concomitant treatment with VEGF and TPO (Fig. 7*A*). The induction of $CD31^{bright}$ cells by these growth factors (Fig. 4*D*) was consistent with the increase in the phosphorylation of Akt at Ser-473. TPO but not VEGF could also stimulate the phosphorylation of STAT3 at Tyr-705. We previously reported that the PI3K/p70 S6 kinase pathway and the JAK/STAT3 pathway were important for proliferation and differentiation, respectively, in neutrophilic differentiation (41, 42). Owing to the stimulation of both the PI3K/Akt and the JAK/STAT pathways, we postulated that TPO may be a stronger stimulator of EPC production than VEGF. As shown in Fig. 7*B*, however, wortmannin could not completely inhibit the induction of $CD31^{bright}$ cells. Therefore, a pathway other than the PI3K/Akt pathway may also work for the proliferation and differentiation of EPCs.

The observation of unfavorable angiogenesis has recently been reported after transplantation of bone marrow mononuclear cells in patients with thromboangiitis obliterans (43). Moreover, transfer of both spleen cell-derived EPCs and bone marrow mononuclear cells accelerate atherosclerosis in apoE knockout mice, whereas EPC transfer reduces markers associated with plaque stability (44). These observations suggest that transplantation of differentiated cells from EPCs may be useful therapy as regenerative medicine.

In conclusion, we have demonstrated a new role of TPO in enhancing the differentiation of $AC133^+$ cells into $CD31^{bright}$ cells (EPCs) *in vitro*. These findings may contribute to further development of cell therapy for critical ischemia.

Acknowledgments—We thank Saitama Red Cross of Japan (Saitama, Japan) and Metro Tokyo Red Cross Cord Blood Bank (Tokyo, Japan) for their kind cooperation. We also thank Kirin-Amgen Inc. for their kind gift of recombinant TPO and recombinant SCF.

REFERENCES

1. Asahara, T., Masuda, H., Takahashi, T., Kalka, C., Pastore, C., Silver, M., Kearne, M., Magner, M., and Isner, J. M. (1999) *Circ. Res.* **85**, 221–228
2. Asahara, T., Murohara, T., Sullivan, A., Silver, M., van der Zee, R., Li, T., Witzenbichler, B., Schatteman, G., and Isner, J. M. (1997) *Science* **275**, 964–967
3. Asahara, T., Takahashi, T., Masuda, H., Kalka, C., Chen, D., Iwaguro, H., Inai, Y., Silver, M., and Isner, J. M. (1999) *EMBO J.* **18**, 3964–3972
4. Shi, Q., Rafii, S., Wu, M. H., Wijelath, E. S., Yu, C., Ishida, A., Fujita, Y., Kothari, S., Mohle, R., Sauvage, L. R., Moore, M. A., Storb, R. F., and Hammond, W. P. (1998) *Blood* **92**, 362–367
5. Takahashi, T., Kalka, C., Masuda, H., Chen, D., Silver, M., Kearney, M., Magner, M., Isner, J. M., and Asahara, T. (1999) *Nat. Med.* **5**, 434–438
6. Nieda, M., Nicol, A., Denning-Kendall, P., Sweetenham, J., Bradley, B., and Hows, J. (1997) *Br. J. Haematol.* **98**, 775–777
7. Gill, M., Dias, S., Hattori, K., Rivera, M. L., Hicklin, D., Witte, L., Girardi, L., Yurt, R., Himel, H., and Rafii, S. (2001) *Circ. Res.* **88**, 167–174
8. Peichev, M., Naiyer, A. J., Pereira, D., Zhu, Z., Lane, W. J., Williams, M.,

Oz, M. C., Hicklin, D. J., Witte, L., Moore, M. A., and Rafii, S. (2000) *Blood* **95,** 952–958
9. Rehman, J., Li, J., Orschell, C. M., and March, K. L. (2003) *Circulation* **107,** 1164–1169
10. Kocher, A. A., Schuster, M. D., Szabolcs, M. J., Takuma, S., Burkhoff, D., Wang, J., Homma, S., Edwards, N. M., and Itescu, S. (2001) *Nat. Med.* **7,** 430–436
11. Bahlmann, F. H., De Groot, K., Spandau, J. M., Landry, A. L., Hertel, B., Duckert, T., Boehm, S. M., Menne, J., Haller, H., and Fliser, D. (2004) *Blood* **103,** 921–926
12. Bahlmann, F. H., DeGroot, K., Duckert, T., Niemczyk, E., Bahlmann, E., Boehm, S. M., Haller, H., and Fliser, D. (2003) *Kidney Int.* **64,** 1648–1652
13. Heeschen, C., Aicher, A., Lehmann, R., Fichtlscherer, S., Vasa, M., Urbich, C., Mildner-Rihm, C., Martin, H., Zeiher, A. M., and Dimmeler, S. (2003) *Blood* **102,** 1340–1346
14. Dimmeler, S., Aicher, A., Vasa, M., Mildner-Rihm, C., Adler, K., Tiemann, M., Rutten, H., Fichtlscherer, S., Martin, H., and Zeiher, A. M. (2001) *J. Clin. Investig.* **108,** 391–397
15. Llevadot, J., Murasawa, S., Kureishi, Y., Uchida, S., Masuda, H., Kawamoto, A., Walsh, K., Isner, J. M., and Asahara, T. (2001) *J. Clin. Investig.* **108,** 399–405
16. Kaushansky, K., Lok, S., Holly, R. D., Broudy, V. C., Lin, N., Bailey, M. C., Forstrom, J. W., Buddle, M. M., Oort, P. J., Hagen, F. S., Roth, G. J., Papayannopoulou, T., and Foster, D. C. (1994) *Nature* **369,** 568–571
17. Fox, N., Priestley, G., Papayannopoulou, T., and Kaushansky, K. (2002) *J. Clin. Investig.* **110,** 389–394
18. Kimura, S., Roberts, A. W., Metcalf, D., and Alexander, W. S. (1998) *Proc. Natl. Acad. Sci. U. S. A.* **95,** 1195–1200
19. Sitnicka, E., Lin, N., Priestley, G. V., Fox, N., Broudy, V. C., Wolf, N. S., and Kaushansky, K. (1996) *Blood* **87,** 4998–5005
20. Brizzi, M. F., Battaglia, E., Montrucchio, G., Dentelli, P., Del Sorbo, L., Garbarino, G., Pegoraro, L., and Camussi, G. (1999) *Circ. Res.* **84,** 785–796
21. Kaushansky, K., Lin, N., Grossmann, A., Humes, J., Sprugel, K. H., and Broudy, V. C. (1996) *Exp. Hematol.* **24,** 265–269
22. Broudy, V. C., Lin, N. L., and Kaushansky, K. (1995) *Blood* **85,** 1719–1726
23. Kaushansky, K., Broudy, V. C., Grossmann, A., Humes, J., Lin, N., Ren, H. P., Bailey, M. C., Papayannopoulou, T., Forstrom, J. W., and Sprugel, K. H. (1995) *J. Clin. Investig.* **96,** 1683–1687
24. Kobayashi, M., Laver, J. H., Kato, T., Miyazaki, H., and Ogawa, M. (1995) *Blood* **86,** 2494–2499
25. Kanayasu-Toyoda, T., Yamaguchi, T., Oshizawa, T., and Hayakawa, T. (2003) *J. Cell. Physiol.* **195,** 119–129
26. Hur, J., Yoon, C. H., Kim, H. S., Choi, J. H., Kang, H. J., Hwang, K. K., Oh, B. H., Lee, M. M., and Park, Y. B. (2004) *Arterioscler. Thromb. Vasc. Biol.* **24,** 288–293
27. Yoon, C. H., Hur, J., Park, K. W., Kim, J. H., Lee, C. S., Oh, I. Y., Kim, T. Y., Cho, H. J., Kang, H. J., Chae, I. H., Yang, H. K., Oh, B. H., Park, Y. B., and Kim, H. S. (2005) *Circulation* **112,** 1618–1627
28. Miyakawa, Y., Rojnuckarin, P., Habib, T., and Kaushansky, K. (2001) *J. Biol. Chem.* **276,** 2494–2502
29. Drachman, J. G., Sabath, D. F., Fox, N. E., and Kaushansky, K. (1997) *Blood* **89,** 483–492
30. Kirito, K., Watanabe, T., Sawada, K., Endo, H., Ozawa, K., and Komatsu, N. (2002) *J. Biol. Chem.* **277,** 8329–8337
31. Li, A., Dubey, S., Varney, M. L., Dave, B. J., and Singh, R. K. (2003) *J. Immunol.* **170,** 3369–3376
32. Mizukami, Y., Jo, W. S., Duerr, E. M., Gala, M., Li, J., Zhang, X., Zimmer, M. A., Iliopoulos, O., Zukerberg, L. R., Kohgo, Y., Lynch, M. P., Rueda, B. R., and Chung, D. C. (2005) *Nat. Med.* **11,** 992–997
33. Salcedo, R., Ponce, M. L., Young, H. A., Wasserman, K., Ward, J. M., Kleinman, H. K., Oppenheim, J. J., and Murphy, W. J. (2000) *Blood* **96,** 34–40
34. Lin, Y., Weisdorf, D. J., Solovey, A., and Hebbel, R. P. (2000) *J. Clin. Investig.* **105,** 71–77
35. Assmus, B., Schachinger, V., Teupe, C., Britten, M., Lehmann, R., Dobert, N., Grunwald, F., Aicher, A., Urbich, C., Martin, H., Hoelzer, D., Dimmeler, S., and Zeiher, A. M. (2002) *Circulation* **106,** 3009–3017
36. Kalka, C., Masuda, H., Takahashi, T., Kalka-Moll, W. M., Silver, M., Kearney, M., Li, T., Isner, J. M., and Asahara, T. (2000) *Proc. Natl. Acad. Sci. U. S. A.* **97,** 3422–3427
37. Kawamoto, A., Gwon, H. C., Iwaguro, H., Yamaguchi, J. I., Uchida, S., Masuda, H., Silver, M., Ma, H., Kearney, M., Isner, J. M., and Asahara, T. (2001) *Circulation* **103,** 634–637
38. Kirito, K., Fox, N., Komatsu, N., and Kaushansky, K. (2005) *Blood* **105,** 4258–4263
39. Kelemen, E., Cserhati, I., and Tanos, B. (1958) *Acta Haematol. (Basel)* **20,** 350–355
40. Yamamoto, S. (1957) *Acta Haematol. Jpn.* **20,** 163
41. Kanayasu-Toyoda, T., Yamaguchi, T., Uchida, E., and Hayakawa, T. (1999) *J. Biol. Chem.* **274,** 25471–25480
42. Yamaguchi, T., Mukasa, T., Uchida, E., Kanayasu-Toyoda, T., and Hayakawa, T. (1999) *J. Biol. Chem.* **274,** 15575–15581
43. Miyamoto, K., Nishigami, K., Nagaya, N., Akutsu, K., Chiku, M., Kamei, M., Soma, T., Miyata, S., Higashi, M., Tanaka, R., Nakatani, T., Nonogi, H., and Takeshita, S. (2006) *Circulation* **114,** 2679–2684
44. George, J., Afek, A., Abashidze, A., Shmilovich, H., Deutsch, V., Kopolovich, J., Miller, H., and Keren, G. (2005) *Arterioscler. Thromb. Vasc. Biol.* **25,** 2636–2641

A Central Role for Nicotinic Cholinergic Regulation of Growth Factor–Induced Endothelial Cell Migration

Martin K.C. Ng, Jenny Wu, Edwin Chang, Bing-yin Wang, Regina Katzenberg-Clark, Akiko Ishii-Watabe, John P. Cooke

Objective—An endothelial nicotinic acetylcholine receptor (nAChR) participates in atherogenesis and tumorigenesis by promoting neovascularization. To date, the mechanisms of nAChR-mediated angiogenesis and their relationship to angiogenic factors, eg, VEGF and bFGF, are unknown.

Methods and Results—Nicotine induced dose-dependent human microvascular endothelial cell (HMVEC) migration, a key angiogenesis event, to an extent which was equivalent in magnitude to bFGF (10 ng/mL) but less than for VEGF (10 ng/mL). Unexpectedly, nAChR antagonism not only abolished nicotine-induced HMVEC migration but also abolished migration induced by bFGF and attenuated migration induced by VEGF. Transcriptional profiling identified gene expression programs which were concordantly regulated by all 3 angiogens (nicotine, VEGF, and bFGF), a notable feature of which includes corepression of thioredoxin-interacting protein (TXNIP), endogenous inhibitor of the redox regulator thioredoxin. Furthermore, TXNIP repression by all 3 angiogens induced thioredoxin activity. Silencing thioredoxin by small interference RNA abrogated all angiogen-induced migration while silencing TXNIP strongly induced HMVEC migration. Interestingly, nAChR antagonism abrogates growth factor (VEGF and bFGF)–mediated induction of thioredoxin activity.

Conclusions—Nicotine promotes angiogenesis via stimulation of nAChR-dependent endothelial cell migration. Furthermore, growth factor–induced HMVEC migration, a key angiogenesis event, requires nAChR activation—an effect mediated in part by nAChR-dependent regulation of thioredoxin activity. (***Arterioscler Thromb Vasc Biol.* 2007;27: 106-112.)**

Key Words: nicotine ■ angiogenesis ■ endothelium ■ vascular endothelial growth factor ■ fibroblast growth factor

The nicotinic acetylcholine receptor (nAChR) is a pentameric ligand-gated cationic channel.[1] The nAChR was first described in neurons, but has recently been identified in many cell types including endothelial cells (ECs) and vascular smooth muscle cells.[2] Intriguingly, ECs also synthesize and store acetylcholine.[3] Recently, we serendipitously discovered that nAChR activation causes ECs to form capillary tubes in vitro, and promotes angiogenesis in vivo.[4,5]

Pathological as well as physiological forms of angiogenesis are mediated by EC nAChRs. For example, by activating the EC nAChR, nicotine accelerates tumor angiogenesis and tumor growth in a murine Lewis lung cancer model.[4] The acceleration of tumor growth by environmental tobacco smoke is also mediated by nAChR-induced angiogenesis.[6] Furthermore, nAChR activation by nicotine stimulates the neovascularization and progression of atherosclerotic plaque.[4] On the other hand, activation of the nAChR in a murine model of diabetic ulceration enhances wound angiogenesis and healing.[7]

To date, the mechanisms of nAChR-mediated angiogenesis and their relationship to established angiogenic growth factors, such as VEGF and bFGF, are unknown. We therefore sought to study and compare the effects of nAChR activation on EC migration, a key event in angiogenesis, alongside those induced by VEGF or bFGF. In this article, we report an unexpected observation: pharmacological antagonism of the nAChR fully blocks bFGF-induced EC migration, and substantially suppresses the endothelial response to VEGF. Furthermore, by microarray analysis, we identify gene expression programs which are concordantly regulated by nicotine, VEGF, or bFGF, and confirm the role of one of these genes in the cholinergic component of growth factor-induced endothelial cell migration.

Methods

For Methods, please refer to the Data Supplement, available online at http://atvb.ahajournals.org.

Original received April 6, 2006; final version accepted October 16, 2006.

From the Department of Medicine (M.K.C.N., J.W., E.C., B.-y.W., R.K.-C., A.I.-W., J.P.C.), Division of Cardiovascular Medicine, Stanford University School of Medicine, Stanford, Calif.; and the Department of Cardiology (M.K.C.N.), Royal Prince Alfred Hospital, Sydney, NSW, Australia.

M.K.C.N. and J.W. contributed equally to this work.

Correspondence to John P. Cooke, Falk Cardiovascular Research Center, Stanford University School of Medicine, 300 Pasteur Drive, Stanford, CA 94305-5406. E-mail john.cooke@stanford.edu

Arterioscler Thromb Vasc Biol. is available at http://www.atvbaha.org

DOI: 10.1161/01.ATV.0000251517.98396.4a

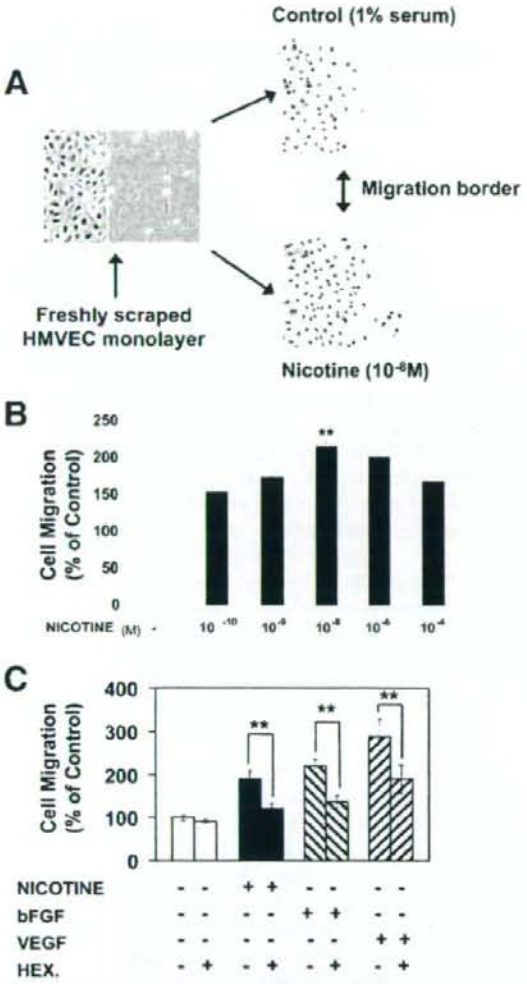

Figure 1. Role of nAChR in human microvascular endothelial cell (HMVEC) migration. A, Representative microphotographs of the HMVEC migration assay: after wounding of the monolayer with a razor blade, HMVECs migrate into the denuded area. B, Nicotine stimulates dose-dependent HMVEC migration which is maximal at a nicotine concentration of 10^{-8} mol/L ($P<0.001$ vs control). C, Effects of hexamethonium (HEX), a nAChR antagonist, on HMVEC migration induced by nicotine (10^{-8} mol/L), VEGF (10 ng/mL), and bFGF (10 ng/mL). Values are expressed as a percentage of migrating cells per high-powered field in vehicle-treated wells. $^{**}P<0.001$.

Results

A Cholinergic Component of Growth Factor–Mediated Endothelial Cell Migration

The effects of nicotine on human microvascular endothelial cell (HMVEC) migration were studied using standard wounding migration assays. Figure 1A depicts typical microphotographs of in vitro HMVEC migration in the presence of vehicle or nicotine. Nicotine stimulated EC migration in a dose-dependent manner with maximal stimulation at 10^{-8} mol/L, producing cell migration that was 216±9% that of vehicle-treated ECs ($P<0.001$ versus control; Figure 1B). Stimulation with VEGF or bFGF also induced EC migration with maximal effects at 10 ng/mL (data not shown). Nicotine-induced EC migration at 10^{-8} mol/L was equivalent in magnitude to that observed for bFGF (10 ng/mL) but less than for VEGF (10 ng/mL; P=NS for nicotine versus bFGF; $P<0.01$ for nicotine versus VEGF; Figure 1C). To further investigate the effects of nAChR-dependent pathways on EC migration, we studied the effect of the nAChR antagonist, hexamethonium (HEX, 10^{-4} mol/L), on EC migration induced by nicotine, VEGF, and bFGF. Hexamethonium abrogated nicotine-induced EC migration (Figure 1C). Unexpectedly, in addition to abolishing NIC-induced EC migration, HEX abolished migration induced by bFGF (P=NS versus control) and reduced migration induced by VEGF ($P<0.01$ for VEGF+HEX versus VEGF alone; Figure 1C). Similar results were observed with the nAChR antagonist, mecamylamine (10^{-6} mol/L; supplemental Figure I). The nAChR-related effect was dose-dependent: in the case of VEGF, cell migration was attenuated by 26±12%, 43±9%, and 52±12% by HEX concentrations of 10^{-8} mol/L, 10^{-6} mol/L, and 10^{-4} mol/L, respectively ($P<0.05$ for trend). Nicotinic receptor activation is known to stimulate EC proliferation.[4] Interestingly, nAChR antagonism also significantly attenuated VEGF- and bFGF-mediated EC proliferation as assessed by bromodeoxyuridine incorporation (supplemental Figure II). The nAChR antagonist-related effects were not the result of cellular toxicity as addition of hexamethonium or mecamylamine alone did not induce cell death as examined via 3-[4,5-dimethylthiazol-2-yl]-2,5-diphenyl tetrazolium bromide (MTT) assays, nor did mecamylamine or hexamethonium induce apoptosis in VEGF- or bFGF-treated cells as assessed by annexin V staining (data not shown).

Previous in vitro and in vivo data have implicated a central role for the α7-nAChR isoform in mediating nAChR-induced neovascularization.[5] Consistent with this, selective inhibition of the α7-nAChR isoform by α-bungarotoxin (10^{-9} mol/L) abrogated nicotine effects (P=NS versus control) and significantly attenuated bFGF and VEGF-induced EC migration by 50±11% and 38±13%, respectively ($P<0.05$ for stimulus versus stimulus + α-bungarotoxin; Figure 2A). We also studied HMVEC α7-nAChR mRNA expression in response to nicotine, VEGF, and bFGF over a 24-hour time course. At 1 hour, nicotine, VEGF, and bFGF all induced >10-fold downregulation of α7-nAChR expression compared with vehicle-treated conditions ($P<0.05$ versus control for all angiogens; Figure 2B). However, by 6 hours, there was significant upregulation of α7-nAChR expression by nicotine (12±0.8-fold), VEGF (11±1.3-fold), and bFGF (4±0.2-fold; $P<0.001$ versus control; Figure 2B). By 24 hours, HMVEC α7-nAChR expression in all conditions had returned to levels similar to control (P=NS versus control). These data suggest that nicotine, VEGF, and bFGF induce acute stimulation of α7-nAChR with subsequent early downregulation of α7-nAChR expression by negative feedback followed by upregulation at 6 hours. These findings are consistent with a role for nAChR in growth factor signaling pathways.

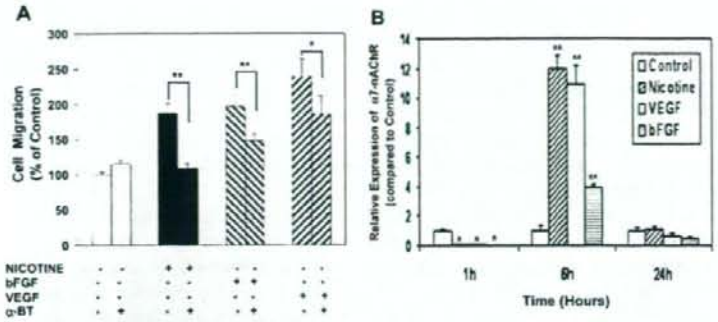

Figure 2. Role of the ∝7-nAChR isoform in growth factor–mediated EC migration. A, Effects of ∝-bungarotoxin (∝-BT), a specific inhibitor of the ∝7-nAChR isoform, on EC migration. Coadministration of ∝-BT (10^{-9} mol/L) abrogated the migragenic effects of nicotine (10^{-6} mol/L; P=NS vs control) and significantly attenuated the effects of bFGF (10 ng/mL) and VEGF (10 ng/mL). B, Effects of nicotine, VEGF, and bFGF on EC ∝7-nAChR expression at 1, 6, and 24 hours as assessed by relative real-time RT-PCR. *P<0.05; **P<0.001 compared with control.

Identification of Shared Transcriptional Responses to Nicotine, bFGF, and VEGF by Microarray Analysis

To further evaluate a cholinergic contribution to growth factor–induced EC migration, and to identify commonly regulated genes that may be required for HMVEC migration, we performed microarray analysis of HMVECs after exposure to nicotine, VEGF, or bFGF. At 24 hours after treatment, each of these stimuli induced profound transcriptional changes in HMVECs (Figure 3), resulting in differential expression of a total of 3072 genes uniquely identified by UniGene, as well as 312 expressed-sequence tags, all of which were represented by 4070 nonredundant cDNA clones. To study relationships between gene expression programs

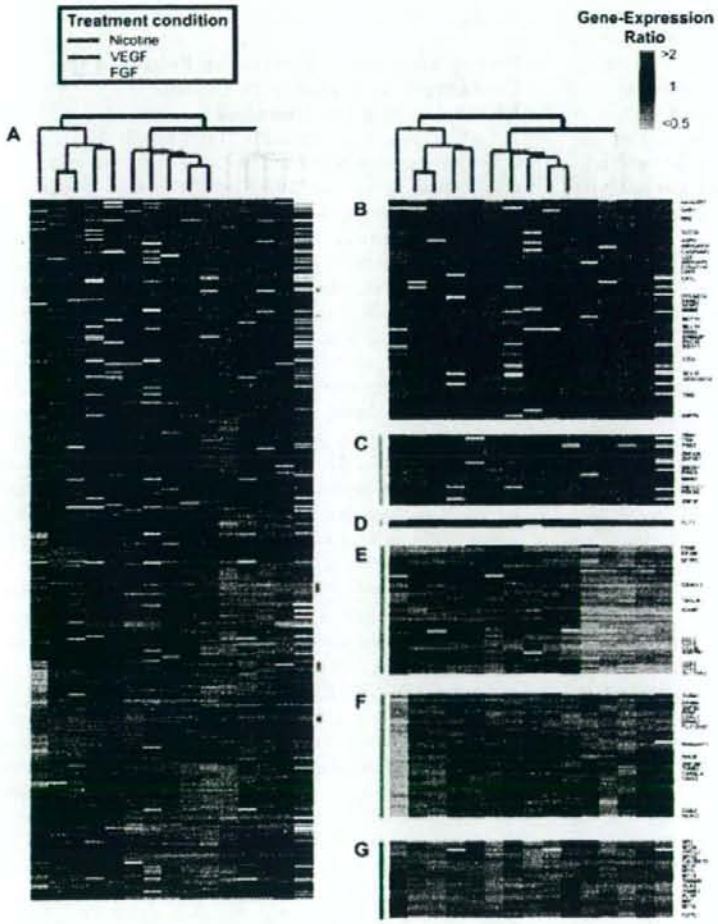

Figure 3. Hierarchical cluster analysis of transcriptional effects of nicotine, VEGF, or bFGF in human microvascular endothelial cells at 24 hours. A, Overview of the two way (genes against conditions) hierarchical cluster of 15 experiments (each condition was studied in quintuplicate) and 4070 nonredundant cDNA clones with significant change in expression at 24 hours. Data from individual elements or genes are represented in rows and experiments in columns. Red and green denote expression levels greater or less, respectively, than control values. Gray denotes technically inadequate or missing data. The intensity of the color reflects the magnitude of the change from baseline. The dendrogram above the matrix represents similarities in patterns of expression between experimental samples. B through G, Zoom boxes of concordantly expressed gene clusters, whose location are indicated by vertical colored bars adjacent to the dendrogram. Owing to space limitations, only genes discussed in the text are indicated by UniGene symbol.

induced by nicotine, VEGF, or bFGF, data for all differentially expressed genes at 24 hours were hierarchically clustered by gene and by array, thereby organizing genes and experimental samples on the basis of similarity of expression patterns (Figure 3A through 3F).[8] The cluster dendrogram shows that all 3 stimuli induced distinct transcriptional signatures which cluster within 3 distinct groups, but there is a closer relationship between the VEGF- and bFGF-induced expression profiles, which cluster together on the same dendrogram branch (Figure 3A).

Within the distinct transcriptional profiles induced by nicotine, VEGF, or bFGF, we identified 6 clusters with concordant gene expression (3 clusters of commonly activated and 3 commonly corepressed genes; Figure 3B through 3F). The characteristics of these clusters provide insights into shared cellular processes that may be requisite for angiogen-induced cell migration. The first activation cluster (Figure 3B), the "migration cluster," was enriched for genes associated with cytokinetic processes including migration-associated G protein signaling (Rho GTPase regulatory proteins and RIN2), integrin binding (ERBB2IP and ADAM9), cell cycle regulation and proliferation (RRM2, MDM2, AHR, MLLT4, and MUTYH), NF-κB activation (BCL10 and CASP8AP2), and migration-associated oxidoreductase activity (LOX and ASPH). Significantly, three Rho GTPase activating proteins (GAPs) including ARHGAP5, ARHGAP21, and ARHGAP24 and one Rho guanine nucleotide exchange factor (GEF), ARHGEF7, were concordantly upregulated in this cluster. Rho GEFs and GAPs, by respectively controlling the activation and inactivation of small Rho GTPases (Cdc42 and Rac), regulate the orchestration of cytoskeletal and adhesive changes during cytokinesis.[9]

A smaller second coactivation cluster (Figure 3C) includes the p21-activated kinase PAK1, an effector for the Rho GTPases Rac and Cdc42, that facilitates cell migration by coordinating formation of new adhesions at the leading edge of the cell with detachment at the trailing edge.[10] Other genes in this activation cluster comprise zinc finger proteins and genes involved in nucleic acid metabolism. Interestingly, all three angiogens induced activation of the VEGF receptor, FLT1, an effect that was stronger for bFGF-treated cells than for nicotine or VEGF (Figure 3D, which contains 3 nonredundant cDNA clones for FLT1). In addition to the coinduction of FLT1 by all three stimuli, we found that several isoforms of nAChR subunits are upregulated by VEGF at 24 hours (supplemental Table I), suggesting other potential synergistic interactions between VEGF and cholinergic signaling pathways.

The first repression cluster (Figure 3E) contains genes that are strongly downregulated by bFGF, many of which are also concordantly repressed by nicotine and VEGF. A dominant theme among concordantly repressed genes is the downregulation of chemokine genes (principally of CC class) involved leukocyte chemotaxis (CCL2, CCL7, CCL8, CCL20, and CX3CL). Another prominent feature is the robust repression of thioredoxin interacting protein (TXNIP) (Figure 3E), a protein that binds and inhibits thioredoxin, a major intracellular antioxidant. Other corepressed genes in this cluster have been implicated in apoptosis (TNFRSF1B, EP300), signal transduction (CD53, SQSTM1), and cell adhesion (ICAM1). The second repression cluster (Figure 3F) included two Ephrin receptors: EPHB4, a marker of venous differentiation and EPHA2, an inhibitor of cell migration which suppresses integrin function. Other genes within this group were associated with tumor suppression, microtubular polymerization, and signal transduction. The striking feature of the third cluster of corepressed genes is a strong enrichment for metallothioneins (MT1E, MT1F, MT1G, MT1L, MT1X, MT2A, and MT3; Figure 3G). Metallothioneins (MTs) comprise a superfamily of small cysteine-rich proteins with high affinity for metal ions and antioxidant activity. By serving as a cellular reservoir for zinc and copper, MTs regulate the function of proteins requiring these metals such as DNA and RNA polymerases, zinc finger transcription factors, and p53.[11] Other genes in this cluster are involved in diverse functions including cell proliferation/apoptosis (MYC, ERCC2), lipid transport (PTLP), calcium ion transport (CACNA1D), and actin binding (COTL1).

In summary, the transcriptional signatures of nicotine, VEGF, and FGF, while distinct, demonstrate many overlapping features. By hierarchical cluster analysis, we have identified a series of shared angiogen-dependent EC transcriptional programs, with implications for understanding shared mechanisms in EC migration/angiogenesis.

Role of Thioredoxin Interacting Protein in the Cholinergic Contribution to Growth Factor–Induced EC Migration

As nAChR antagonism modulates VEGF- and bFGF-dependent EC migration, we hypothesized that some of the transcriptional effects shared by nicotine, VEGF, and bFGF may be nAChR-dependent. Thioredoxin interacting protein (TXNIP), a gene not previously associated with EC migration, was downregulated by all three angiogens. TXNIP is the endogenous inhibitor of thioredoxin. Thioredoxin is a major redox regulator of protein function increasingly implicated in tumorigenesis.[12,13] In microarray data from 3 nonredundant cDNA clones for TXNIP, nicotine, VEGF, and bFGF consistently decreased TXNIP expression—a finding confirmed by RT-PCR, which demonstrated decreased expression by 42±4%, 33±6%, and 26±7% relative to control, respectively ($P<0.001$ for all stimuli; Figure 4A). As in vivo reduction of TXNIP expression in the order of 30% to 40% has been associated with >3-fold increases in thioredoxin activity,[14] we hypothesized that TXNIP downregulation may influence thioredoxin activity and play a role in angiogen-mediated EC migration.

Using a standard assay for thioredoxin activity,[15] we found that addition of nicotine or VEGF induced thioredoxin activity significantly above vehicle-treated cells ($P<0.001$ versus control for all stimuli; Figure 4B). The addition of bFGF induced a less robust ($P<0.05$ versus control) but significant increase in thioredoxin activity (Figure 4B). Notably, coadministration of hexamethonium inhibited nicotine-, VEGF-, or bFGF-induced thioredoxin activity (Figure 4B: $P<0.001$ for each stimulus versus stimulus + hexamethonium). Hexamethonium alone had no significant effect on thioredoxin activity. Consistent with these results, nAChR antagonism abrogated nicotine, VEGF, and bFGF-mediated repression of TXNIP mRNA expression (P=NS versus control for each stimulus + hexamethonium; Figure 4A). Transfection of small interference RNA (siRNA)

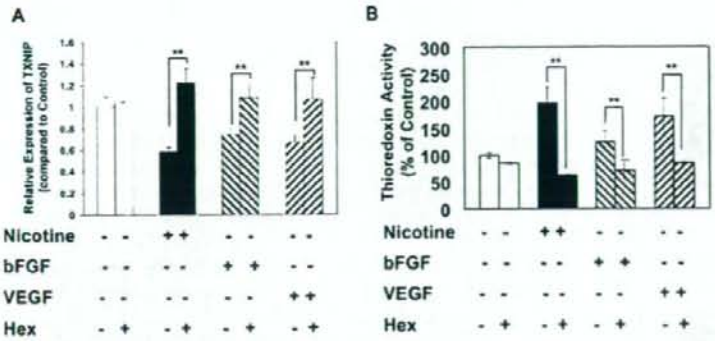

Figure 4. Role of nAChR in growth factor–mediated regulation of TXNIP expression and thioredoxin activity in ECs. Effects of nicotine (10^{-8} mol/L), VEGF (10 ng/mL), and bFGF (10 ng/mL) with/without coadministration of hexamethonium (10^{-4} mol/L) on TXNIP expression (A) and on thioredoxin activity (B) in human microvascular endothelial cells. Values for thioredoxin activity are expressed as a percentage of control (vehicle-treated cells). $^{**}P<0.01$.

against thioredoxin abrogated nicotine-, VEGF-, or bFGF-induced thioredoxin activity and abolished cell migration induced by nicotine, VEGF, or bFGF (P=NS versus control for each stimulus + siRNA; Figure 5A and 5B). Furthermore, in the absence of angiogenic stimuli, siRNA against TXNIP significantly stimulated thioredoxin activity ($P<0.0001$ versus control; Figure 6A) and strongly stimulated HMVEC migration (Figure 6B, $P<0.0001$ versus control). These studies indicate that inhibition of TXNIP by cholinergic or growth factor activation promotes endothelial cell migration, via derepression of thioredoxin activity. Furthermore, VEGF- or bFGF-mediated regulation of TXNIP expression is dependent on activation of nAChR (Figure 4A).

Discussion

We report a cholinergic contribution to growth factor-induced endothelial cell migration. The salient observations are that: (1) activation of nAChR induces EC migration similar in magnitude to that observed for bFGF or VEGF; (2) antagonism of nAChR markedly attenuates the migragenic effects of bFGF or VEGF on ECs; (3) the nAChR-dependent effects of bFGF and VEGF on EC migration are due, in large part, to activation of the α7-nAChR isoform; (4) nAChR activation induces a transcriptional profile that has many overlapping features to those induced by bFGF or VEGF, particularly for genes involved in EC migration; (5) downregulation of TXNIP with subsequent induction of thioredoxin activity is shown to be important to the migragenic effects exerted by each of the stimuli; (6) antagonism of the nAChR abrogates VEGF- or bFGF-mediated regulation of TXNIP expression. In toto, our findings identify a novel role for the nicotinic cholinergic pathway in growth factor-mediated EC migration, a critical event in angiogenesis.

Previous studies have demonstrated that ECs synthesize, store, and release acetylcholine[16] and express functional nAChRs.[2] Increasing evidence suggests that such nonneuronal nAChRs are involved in the regulation of vital cell functions, such as mitosis, differentiation, organization of the cytoskeleton, cell–cell contact, locomotion, and migration.[17] Thus, acetylcholine, originally identified as a neurotransmitter, may function as an autocrine factor that modulates migration of endothelial cells. We and others have previously shown that exogenous nicotine, at pathophysiologically relevant concentrations, promotes angiogenesis in a number of in vivo settings, including inflammation, wound healing, ischemia, tumor, and atherosclerosis.[4,7,18] Furthermore, inhibition of nAChR, in the absence of exogenous nicotine, reduces the angiogenic response in vitro and in vivo, indicating that there exists an endogenous cholinergic pathway for angiogenesis.[5] In contrast, recent work has shown that VEGF and FGF, originally identified as angiogenic growth factors, exert neurotrophic effects and promote neurogenesis.[19,20] These and other data suggest that there may be interdependence between "vascular" and "neuronal" factors and processes.

In this study, we found that nicotine induced dose-dependent nAChR-mediated EC migration which was maximal at concentrations consistent with those found in moderate smokers (10^{-8} mol/L). Surprisingly, coadministration of nAChR antagonists, hexamethonium, or mecamylamine, significantly attenuated the migragenic response of ECs to both VEGF and bFGF. Although several nAChR isoforms exist, we have previously identified a principal role for the α7-nAChR isoform in nAChR-mediated

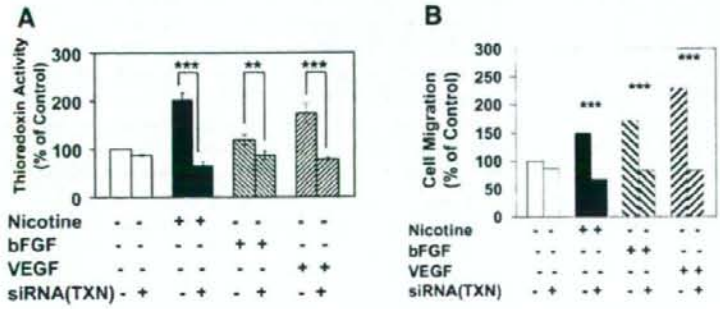

Figure 5. Effects of gene knockdown of thioredoxin by small interference RNA (siRNA) on induction of thioredoxin activity in human microvascular endothelial cells (HMVECs) by nicotine (10^{-8} mol/L), VEGF(10 ng/mL), or bFGF (10 ng/mL) (A) and HMVEC migration induced by nicotine, VEGF, or bFGF (B). Scrambled (randomly arranged) siRNA had no effect on thioredoxin activity or HMVEC migration (data not shown). Values for thioredoxin activity and migration are expressed as a percentage of control (vehicle-treated cells). TXN indicates thioredoxin. $^{**}P=0.01$; $^{***}P<0.001$.

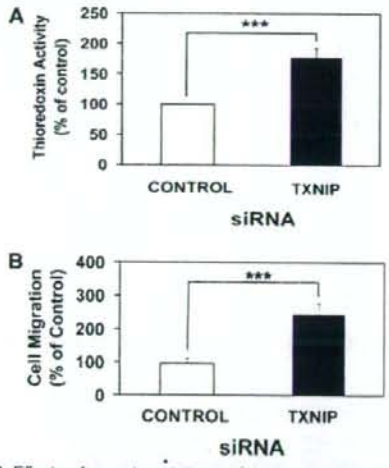

Figure 6. Effects of gene knockdown of thioredoxin interacting protein (TXNIP) by small interference RNA (siRNA) on thioredoxin activity (A) and human microvascular endothelial cell (HMVEC) migration (B). Scrambled (randomly arranged) siRNA had no effect on thioredoxin activity or HMVEC migration (data not shown). Values for thioredoxin activity and migration are expressed as a percentage of control (vehicle-treated cells). ***$P<0.0001$.

angiogenesis in vitro and in vivo.[5] Consistent with these findings, we now find that VEGF and bFGF both induced changes in α7-nAChR expression consistent with activation of α7-nAChR. Moreover, the α7-nAChR selective antagonist, α-bungarotoxin, attenuated VEGF and bFGF-induced EC migration to a similar extent as for the nonselective antagonists, hexamethonium, and mecamylamine. These latter findings suggest that nAChR-dependent pathways, particularly via α7-nAChR activation, are involved in the modulation of growth factor–induced EC migration.

To study the relationship between nicotine and angiogenic growth factors at a genomic level, microarray analysis was performed after HMVEC exposure to nicotine, VEGF, or bFGF. By hierarchical clustering, we found that each stimulus induced distinct but overlapping transcriptional responses, with concordant gene expression being concentrated within six largely functionally coherent gene clusters. A major functional theme among concordantly expressed genes was the coregulation of cell motility-related processes by all three angiogens. In particular, a "migration" cluster of concordantly activated genes was strongly enriched for genes involved in cytokinetic-related processes such as the Rho GTPase cell motility pathways, integrin binding, cell cycle regulation, and NF-κB activation. Our findings with regard to activation of Rho GTPase pathways by VEGF and bFGF are consistent with previous studies[21] and reinforce the central role of Rho-related regulation of actomyosin cytoskeletal organization EC migration during angiogenesis. We previously demonstrated that nAChR-dependent endothelial tube formation in vitro is dependent on NF-κB activation.[5] The migration cluster included two genes associated with NF-κB activation: BCL10, an important activator of NF-κB downstream of protein kinase C, and CASP8AP2 (aka FLASH), which coordinates downstream NF-κB activity via a TRAF2-dependent pathway.[22] In addition, many genes within the migration cluster have been implicated in oncogenesis (MDM2, ADAM9, BCL10, etc), a finding pathogenetically consistent with the role of angiogenesis in cancer.

The majority of concordantly regulated genes revealed by our microarray analyses have not been previously associated with angiogenesis. These include the p53 inhibitor MDM2 (activated by all three stimuli) and TXNIP, C-C chemokines, and metallothioneins (repressed by all three stimuli). These concordant transcriptional profiles provide further evidence for a cholinergic component of the angiogenic pathways. For example, our findings of coinduction of FLT1 by all three stimuli, and of nAChR subunit induction by VEGF are consistent with interaction between the signaling pathways.

Of the coregulated genes identified by hierarchical clustering, we focused our attention on TXNIP. Originally identified in HL-60 leukemia cells treated with 1,25 dihydroxyvitamin D_3 (and previously known as Vitamin D_3 upregulated protein 1), TXNIP is an endogenous inhibitor of the ubiquitous redox protein thioredoxin.[12] Thioredoxin, a major redox regulator of protein function and signaling via thiol redox control, has been implicated in the regulation of cellular responses to oxidative stress and apoptosis.[23] Thioredoxin selectively regulates the activity of DNA-binding proteins; for example, two transcription factors concordantly regulated by the three stimuli, NF-κB, and p53, require thioredoxin reduction for stimulation of DNA binding.[23,24] Increasing evidence implicates TXNIP and thioredoxin in tumorigenesis. Thioredoxin expression is increased in several human primary cancers, whereas TXNIP is strongly downregulated in human tumor tissues.[13,25] Inhibition of thioredoxin signaling with experimental antitumor agents such as PX-12 (1-methylpropyl 2-imidazolyl disulfide) and pleurotin reduces tumor cell production of HIF-1α and VEGF in vitro and inhibits tumor angiogenesis in vivo.[26] We hypothesized that repression of TXNIP may play a role in mediating growth factor–mediated EC migration.

In the present study, we found that nicotine, VEGF, and bFGF stimulated thioredoxin activity—a finding consistent with their common suppression of TXNIP. Gene knockdown of thioredoxin by siRNA reversed the effect of growth factor stimulation and abrogated the effect of nicotine, VEGF, or bFGF on EC migration. These findings are consistent with a critical role for thioredoxin in mediating growth factor–induced EC migration. Interestingly, the increase in thioredoxin activty induced by each of the three stimuli could be blocked by nAChR antagonism. Finally, gene knockdown of TXNIP alone, without addition of growth factors, induced EC migration. Our findings indicate that TXNIP, by regulating of thioredoxin activity, may play an important role in angiogenesis mediated by growth factor receptors or nAChRs. The mechanism whereby thioredoxin mediates EC migration is poorly understood but may involve stimulation of hypoxia-inducible factor-1α (HIF-1α), a transcription factor that plays a central role in mediating the angiogenic response to hypoxia. Overexpression of thioredoxin in a variety of malignant cells has been shown to induce HIF-1α expression and VEGF production.[27] Induction of HIF-1α in human endothelial cells upregulates the expression of multiple angiogenic factors including the angiopoietins which are potent stimulators of cell migration via Tie-2 signal transduction pathways.[28] Moreover, as cellular redox state is an important determinant of Rho

GTPase activity, it is possible that thioredoxin may play a role in Rho-mediated cytoskeletal remodelling during cell migration.[29]

In summary, our data show that activation of nicotinic acetylcholine receptors (nAChRs) induces endothelial cell migration. Furthermore, growth factor (VEGF and bFGF)–induced endothelial cell migration involves nAChR activation. By transcriptional profiling we have identified convergent genomic responses of ECs to nicotine, VEGF, and bFGF. Identification of concordantly regulated genes may provide novel insights into molecular processes mediating EC migration and angiogenesis. Indeed, using this approach we found that TXNIP, by regulating thioredoxin activity, is centrally involved in nAChR-mediated EC migration. Our studies provide evidence for a cholinergic contribution to growth factor-induced EC migration. The nAChRs may play an important role in growth factor-induced angiogenesis, and thus may be a target for therapeutic modulation in disorders of pathological or insufficient angiogenesis.

Acknowledgments

We thank Mary Gerritsen, PhD, and Ken Kengatharan, PhD for scientific and editorial comments.

Sources of Funding

Akiko Ishii-Watabe is supported by the Japanese Health Sciences Foundation. Martin K.C. Ng is supported by the National Health and Medical Research Council of Australia. This study was supported by grants from the National Institutes of Health (R01 HL-63685; RO1 HL-75774; R01 CA098303 and P01 AG18784; and PO1A150153); Philip Morris USA Inc; and the Tobacco Related Disease Research Program (11RT-0147).

Disclosures

Dr Cooke holds equity in Athenagen Inc, which has licensed Stanford University patents for the use of nAChR agonists and antagonists for disorders of angiogenesis. Dr Cooke is an inventor on these patents, and receives royalties from the licenses. A patent is being filed based upon the intellectual property described in this manuscript that may benefit J.P.C., M.K.C.N., E.C., and J.W.

References

1. Lindstrom J. Nicotinic acetylcholine receptors in health and disease. *Mol Neurobiol*. 1997;15:193–222.
2. Macklin KD, Maus AD, Pereira EF, Albuquerque EX, Conti-Fine BM. Human vascular endothelial cells express functional nicotinic acetylcholine receptors. *J Pharmacol Exp Ther*. 1998;287:435–439.
3. Parnavelas JG, Kelly W, Burnstock G. Ultrastructural localization of choline acetyltransferase in vascular endothelial cells in rat brain. *Nature*. 1985;316:724–725.
4. Heeschen C, Jang JJ, Weis M, Pathak A, Kaji S, Hu RS, Tsao PS, Johnson FL, Cooke JP. Nicotine stimulates angiogenesis and promotes tumor growth and atherosclerosis. *Nat Med*. 2001;7:833–839.
5. Heeschen C, Weis M, Aicher A, Dimmeler S, Cooke JP. A novel angiogenic pathway mediated by non-neuronal nicotinic acetylcholine receptors. *J Clin Invest*. 2002;110:527–536.
6. Zhu BQ, Heeschen C, Sievers RE, Karliner JS, Parmley WW, Glantz SA, Cooke JP. Second hand smoke stimulates tumor angiogenesis and growth. *Cancer Cell*. 2003;4:191–196.
7. Jacobi J, Jang J, Sundram U, Dayoub H, Fajardo LF, Cooke JP. Nicotine accelerates angiogenesis and wound healing in genetically diabetic mice. *Am J Pathol*. 2002;161:97–104.
8. Eisen MB, Spellman PT, Brown PO, Botstein D. Cluster analysis and display of genome-wide expression patterns. *Proc Natl Acad Sci U S A*. 1998;95:14863–14868.
9. Ridley A, Schwartz M, Burridge K, Firtel R, Ginsberg M, Borisy G, Parsons J, Horwitz A. Cell migration: integrating signals from front to back. *Science*. 2003;302:1704–1709.
10. Kiosses W, Daniels R, Otey C, Bokoch G, Schwartz M. A role for p21-activated kinase in endothelial cell migration. *J Cell Biol*. 1999;147:831–844.
11. Henkel G, Krebs B. Metallothioneins: zinc, cadmium, mercury, and copper thiolates and selenolates mimicking protein active site features - structural aspects and biological implications. *Chem Rev*. 2004;104:801–824.
12. Nishiyama A, Matsui M, Iwata S, Hirota K, Masutani H, Nakamura H, Takagi Y, Sono H, Gon Y, Yodoi J. Identification of thioredoxin-binding protein-2/vitamin D(3) up-regulated protein 1 as a negative regulator of thioredoxin function and expression. *J Biol Chem*. 1999;274:21645–21650.
13. Baker A, Payne CM, Briehl MM, Powis G. Thioredoxin, a gene found overexpressed in human cancer, inhibits apoptosis *in vitro* and *in vivo*. *Cancer Res*. 1997;57:5162–5167.
14. Yoshioka J, Schulze PC, Cupesi M, Sylvan JD, MacGillivray C, Gannon J, Huang H, Lee RT. Thioredoxin-interacting protein controls cardiac hypertrophy through regulation of thioredoxin activity. *Circulation*. 2004;109:2581–2586.
15. Wang YG, De Keulenaer GW, Lee RT. Vitamin D(3)-up-regulated protein-1 is a stress-responsive gene that regulates cardiomyocyte viability through interaction with thioredoxin. *J Biol Chem*. 2002;277:26496–26500.
16. Milner P, Kirkpatrick KA, Ralevic V, Toothill V, Pearson J, Burnstock G. Endothelial cells cultured from human umbilical vein release ATP, substance P and acetylcholine in response to increased flow. *Proc Biol Sci*. 1990;241:245–248.
17. Wessler I, Kirkpatrick CJ, Racke K. The cholinergic 'pitfall': acetylcholine, a universal cell molecule in biological systems, including humans. *Clin Exp Pharmacol Physiol*. 1999;26:198–205.
18. Natori T, Sata M, Washida M, Hirata Y, Nagai R, Makuuchi M. Nicotine enhances neovascularization and promotes tumor growth. *Mol Cells*. 2003;16:143–146.
19. Jin K, Zhu Y, Sun Y, Mao XO, Xie L, Greenberg DA. Vascular endothelial growth factor (VEGF) stimulates neurogenesis in vitro and in vivo. *Proc Natl Acad Sci U S A*. 2002;99:11946–11950.
20. Yoshimura S, Takagi Y, Harada J, Teramoto T, Thomas SS, Waeber C, Bakowska JC, Breakefield XO, Moskowitz MA. FGF-2 regulation of neurogenesis in adult hippocampus after brain injury. *Proc Natl Acad Sci U S A*. 2001;10:5874–5879.
21. Soga N, Namba N, McAllister S, Cornelius L, Teitelbaum S, Dowdy S, Kawamura J, Hruska K. Rho family GTPases regulate VEGF-stimulated endothelial cell motility. *Exp Cell Res*. 2001;269:73–87.
22. Choi Y, Kim K, Kim H, Hong G, Kwon Y, Chung C, Park Y, Shen Z, Kim B, Lee S, Jung Y. FLASH coordinates NF-kappa B activity via TRAF2. *J Biol Chem*. 2001;276:25073–25077.
23. Yamawaki H, Haendeler J, Berk BC. Thioredoxin: A key regulator of cardiovascular homeostasis. *Circ Res*. 2003;93:1029–1033.
24. Ueno M, Masutani H, Arai RJ, Yamauchi A, Hirota K, Sakai T, Inamoto T, Yamaoka Y, Yodoi J, Nikaido T. Thioredoxin-dependent redox regulation of p53-mediated p21 activation. *J Biol Chem*. 1999;274:35809–35815.
25. Kakolyris S, Giatromanolaki A, Koukourakis M, Powis G, Souglakos J, Sivridis E, Georgoulias V, Gatter KC, Harris AL. Thioredoxin expression is associated with lymph node status and prognosis in early operable non-small cell lung cancer. *Clin Cancer Res*. 2001;7:3087–3091.
26. Welsh SJ, Williams RR, Birmingham A, Newman DJ, Kirkpatrick DL, Powis G. The thioredoxin redox inhibitors 1-methylpropyl 2-imidazolyl disulfide and pleurotin inhibit hypoxia-induced factor 1alpha and vascular endothelial growth factor formation. *Mol Cancer Ther*. 2003;2:235–243.
27. Welsh SJ, Bellamy WT, Briehl MM, Powis G. The redox protein thioredoxin-1 (Trx-1) increases hypoxia-inducible factor 1alpha protein expression: Trx-1 overexpression results in increased vascular endothelial growth factor production and enhanced tumor angiogenesis. *Cancer Res*. 2002;62:5089–5095.
28. Yamakawa M, Liu LX, Date T, Belanger AJ, Vincent KA, Akita GY, Kuriyama T, Cheng SH, Gregory RJ, Jiang C. Hypoxia-inducible factor-1 mediates activation of cultured vascular endothelial cells by inducing multiple angiogenic factors. *Circ Res*. 2003;93:664–673.
29. Nimnual AS, Taylor LJ, Bar-Sagi D. Redox-dependent downregulation of Rho by Rac. *Nat Cell Biol*. 2003;5:236–241.

Miscibility of Nifedipine and Hydrophilic Polymers as Measured by ^{1}H-NMR Spin–Lattice Relaxation

Yukio Aso,*[a] Sumie Yoshioka,[a] Tamaki Miyazaki,[a] Tohru Kawanishi,[a] Kazuyuki Tanaka,[b] Satoshi Kitamura,[b] Asako Takakura,[c] Takashi Hayashi,[c] and Noriyuki Muranushi[c]

[a] National Institute of Health Sciences; 1–18–1 Kamiyoga, Setagaya-ku, Tokyo 158–8501, Japan: [b] Astellas Pharma Inc.; 180 Ozumi, Yaizu, Shizuoka 425–0072, Japan: and [c] Shionogi & Co., Ltd.; 2–1–3 Kuise, Terajima, Amagasaki, Hyogo 660–0813, Japan. Received April 19, 2007; accepted June 4, 2007; published online June 5, 2007

The miscibility of a drug with excipients in solid dispersions is considered to be one of the most important factors for preparation of stable amorphous solid dispersions. The purpose of the present study was to elucidate the feasibility of ^{1}H-NMR spin–lattice relaxation measurements to assess the miscibility of a drug with excipients. Solid dispersions of nifedipine with the hydrophilic polymers poly(vinylpyrrolidone) (PVP), hydroxypropylmethylcellulose (HPMC) and α,β-poly(*N*-5-hydroxypentyl)-L-aspartamide (PHPA) with various weight ratios were prepared by spray drying, and the spin–lattice relaxation decay of the solid dispersions in a laboratory frame (T_1 decay) and in a rotating frame ($T_{1\rho}$ decay) were measured. $T_{1\rho}$ decay of nifedipine–PVP solid dispersions (3 : 7, 5 : 5 and 7 : 3) was describable with a mono-exponential equation, whereas $T_{1\rho}$ decay of nifedipine–PHPA solid dispersions (3 : 7, 4 : 6 and 5 : 5) was describable with a bi-exponential equation. Because a mono-exponential $T_{1\rho}$ decay indicates that the domain sizes of nifedipine and polymer in solid dispersion are less than several nm, it is speculated that nifedipine is miscible with PVP but not miscible with PHPA. All the nifedipine–PVP solid dispersions studied showed a single glass transition temperature (T_g), whereas two glass transitions were observed for the nifedipine–PHPA solid dispersion (3 : 7), thus supporting the above speculation. For nifedipine–HPMC solid dispersions (3 : 7 and 5 : 5), the miscibility of nifedipine and HPMC could not be determined by DSC measurements due to the lack of obviously evident T_g. In contrast, ^{1}H-NMR spin–lattice relaxation measurements showed that nifedipine and HPMC are miscible, since $T_{1\rho}$ decay of the solid dispersions (3 : 7, 5 : 5 and 7 : 3) was describable with a mono-exponential equation. These results indicate that ^{1}H-NMR spin–lattice relaxation measurements are useful for assessing the miscibility of a drug and an excipient in solid dispersions.

Key words miscibility; solid dispersion; spin diffusion; spin–lattice relaxation time; amorphous

Preparing solid dispersions of a poorly soluble drug with water-soluble polymers is a promising method for improving the dissolution characteristics and bioavailability of the drug. Miscibility between a drug and a polymer is considered to be one of the most important factors for obtaining stable solid dispersions.[1)]

Miscibility of a drug with a polymer is usually evaluated by differential scanning calorimetry (DSC).[2—6)] When a solid dispersion shows a single glass transition temperature (T_g) between the T_g values of the drug and the polymer, the drug and the polymer are considered to be miscible within the detection limit of DSC.[7)] This method is applicable to a solid dispersion when T_g of the drug and the polymer can be detected clearly, and the temperature ranges of the base line shift due to glass transition do not overlap each other.

The interaction parameter χ of the Flory–Huggins equation provides a measure of miscibility.[8,9)] Crowly and Zografi measured the water vapor sorption isotherm of indomethacin solid dispersions with PVP and reported that the estimated interaction parameter χ between indomethacin and PVP was greater than 0.5, indicating that indomethacin and PVP are immiscible in terms of χ value.[8)] Although this method is excellent in being able to provide a quantitative measure of miscibility, it may be difficult to apply to unstable amorphous drugs, which crystallize during measurement of water vapor sorption.

A method that can be used as an alternative to DSC or measurement of the interaction parameter χ is analysis of the ^{1}H spin–lattice relaxation process of solid dispersions, which has been reported in the fields of polymer alloy and polymer blends. If two polymers are miscible, the relaxation decay of the mixture is describable by a mono-exponential equation, whereas if they are not miscible, relaxation decay is describable by a bi-exponential equation.[10,11)]

In this paper, the feasibility of ^{1}H spin–lattice relaxation measurements for evaluating the miscibility of a drug and polymers in solid dispersions was studied. Nifedipine solid dispersions with PVP, HPMC and α,β-poly(*N*-5-hydroxypentyl)-L-aspartamide (PHPA) were used as model solid dispersions, and the miscibility measured by ^{1}H-NMR was compared with that measured by DSC. The dissolution profiles of nifedipine from PVP solid dispersions were compared with those from PHPA solid dispersions to discuss the effects of miscibility on the dissolution rate of nifedipine.

Theory ^{1}H spin–lattice relaxation rates of respective spins in a solid are usually averaged by a process called spin diffusion. Spin diffusion is the equilibration process of polarizations of spins at different local sites through mutual exchange of magnetization. ^{1}H spin–lattice relaxation decay for a single-phase solid is describable by a mono-exponential equation with a relaxation rate that is averaged by spin diffusion. When a solid consists of two phases, the spin–lattice relaxation decay is describable by a mono-exponential or a bi-exponential equation depending on both the domain size of each phase and the effective diffusion length (L). L is expressed as follows:

$$L=\sqrt{6Dt} \quad (1)$$

* To whom correspondence should be addressed. e-mail: aso@nihs.go.jp

where D is the spin diffusion coefficient, and t is the diffusion time. D is a function of the distance between neighboring proton spins and spin–spin relaxation time (T_2), and is reported to be approximately 10^{-12} cm^2 s^{-1} for organic polymers. Typical spin–lattice relaxation time in a laboratory frame (T_1) and that in a rotating frame ($T_{1\rho}$) are of the order of 1 s and 10 ms, respectively. When these values for t were inserted in Eq. 1, effective diffusion lengths of approximately 50 nm and 5 nm were obtained for T_1 and $T_{1\rho}$, respectively. Depending on the domain size of each phase in a solid, the following 3 cases can be expected: (1) when the domain is smaller than about 5 nm, both the spin–lattice relaxation decay patterns in a laboratory frame (T_1 decay) and in a rotating frame ($T_{1\rho}$ decay) are describable by a mono-exponential equation; (2) when the domain size is about 5 to 50 nm, the $T_{1\rho}$ decay pattern is describable by a bi-exponential equation, whereas the T_1 decay pattern is describable by a mono-exponential equation; and (3) when the domain size is larger than about 50 nm, both the T_1 and $T_{1\rho}$ decay patterns are describable by a bi-exponential equation. When the $T_{1\rho}$ decay is describable by a mono-exponential equation, the solid can be considered as a single phase within the detection limit of NMR. T_1 and $T_{1\rho}$ decay thus provide information on miscibility of a drug and a polymer excipient.[11]

Experimental

Materials Nifedipine (N-7634), PVP (PVP-40) and HPMC (H-3785) were purchased from Sigma (Newcastle, DE, U.S.A.). PHPA was synthesized *via* polycondensation of L-aspartic acid.[12] Phenobarbital was obtained from sodium phenobarbital (Wako Pure Chemical Ind., Osaka) by neutralization and subsequent re-crystallization from acetone solutions as described previously.[13] Other chemicals used were of reagent grade. Nifedipine solid dispersions with PVP, HPMC and PHPA were prepared by a solvent evaporation method using a model GS-310 spray dryer (Yamato, Tokyo, Japan). Drying conditions are summarized in Table 1. The solid dispersions obtained were confirmed to be amorphous from microscopic observation under polarized light. Although the drying conditions were not optimized, 50 to 90% of the solid dispersions were obtained. Amorphous nifedipine was prepared by melting and subsequent rapid cooling as reported previously.[14]

DSC T_g of nifedipine–PVP and nifedipine–HPMC solid dispersions was measured by modulated temperature DSC using a model 2920 differential scanning calorimeter and a refrigerator cooling system (TA Instruments, Newcastle, DE, U.S.A.). The modulated temperature program used was a modulation amplitude of ±0.5 °C, a modulation period of 100 s and an underlying heating rate of 1 °C/min. For nifedipine–PHPA solid dispersions, T_g was measured at a scanning rate of 20 °C/min using a conventional heating program. Temperature calibration of the instrument was carried out using indium.

NMR T_1 decay and $T_{1\rho}$ decay were measured using a model JNM-MU25 pulsed NMR spectrometer (JEOL DATUM, Tokyo, Japan). The inversion recovery pulse sequence was used to measure T_1 decay. $T_{1\rho}$ decay was measured in a spin locking field of 10 G. All measurements were carried out at 27 °C.

X-Ray Powder Diffraction X-Ray powder diffraction patterns of solid dispersions were obtained using a model RINT-TTR II X-ray diffractometer (Rigaku Denki, Tokyo) with Cu$K\alpha$ radiation (50 kV, 300 mA) at a scanning rate of 4 °C/min from 2θ=5° to 40°.

Nifedipine Dissolution Profile Nifedipine–PVP (3 : 7) and nifedipine–PHPA (3 : 7) solid dispersions containing 100 mg of nifedipine were made into disks with a diameter of 2 cm at a pressure of 20 kN. Each disk was mounted on the rotor of the dissolution apparatus and the side surface of the disk was covered with a Teflon film. The sample was rotated at a rate of 100 rpm in 900 ml of distilled water at 37 °C. The amount of nifedipine dissolved was measured using a model DM-3100 solution monitor (Otsuka Electronics, Tokyo).

Results and Discussion

Figure 1 shows typical T_1 and $T_{1\rho}$ decay patterns for the solid dispersion and the physical mixture of nifedipine and PHPA (3 : 7). T_1 and $T_{1\rho}$ decay patterns were mono-exponential for both amorphous nifedipine and PHPA. The T_1 and $T_{1\rho}$ values of nifedipine were 5.0 s and 104 ms, respectively, and those of PHPA were 0.084 s and 4.4 ms, respectively. The physical mixture of nifedipine and PHPA (3 : 7) exhibited bi-exponential T_1 and $T_{1\rho}$ decay with the relaxation time of each component, indicating that the particle sizes of nifedipine and PHPA in the physical mixture are much larger than the effective diffusion length (approximately 5 nm and 50 nm for $T_{1\rho}$ and T_1 decay, respectively). In contrast to the physical

Table 1. Conditions of Spray Drying

Drug	Polymer	Solvent[a]	Outlet temperature (°C)	Atomizer gas (l/min)	Feeding rate (ml/min)
Nifedipine–PHPA					
0	10	A	68	7	5
3	7	A	68	7	3
4	6	A	68	7	3
5	5	A	68	7	3
Phenobarbital–PHPA					
3	7	A	68	7	3
Nifedipine–PVP					
0	10	A	90	9	10
3	7	A	90	9	10
5	5	A	90	9	10
7	3	A	68	7	3
Nifedipine–HPMC					
0	10	B	38	11	3
3	7	B	38	11	2
5	5	B	38	11	2
7	3	B	38	11	4

a) Solvent A, ethanol; solvent B, ethanol–CH_2Cl_2 (1 : 1). Flow rate of drying gas was adjusted to 0.5 m^3/min.

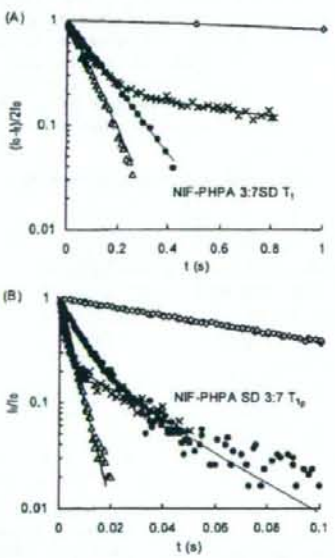

Fig. 1. T_1 (A) and $T_{1\rho}$ (B) Decay Patterns for Amorphous Nifedipine (◇), Amorphous PHPA (△), Physical Mixture (×) and Solid Dispersions (●) of Nifedipine and PHPA

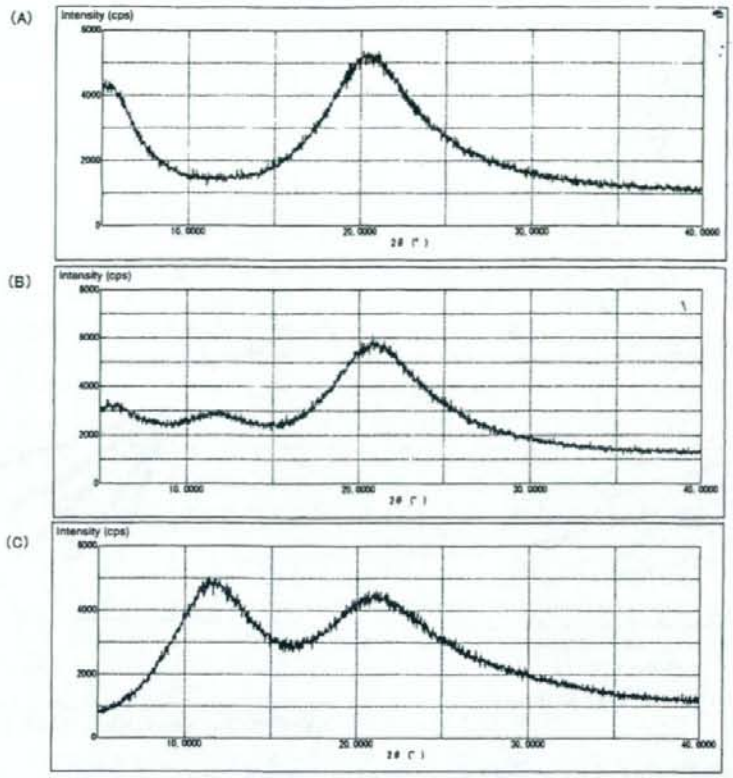

Fig. 2. Powder X-Ray Diffraction Patterns of PHPA (A), Nifedipine–PHPA (3 : 7) (B) and Nifedipine–PVP Solid Dispersions (3 : 7) (C)

mixture, the solid dispersion (3 : 7) showed mono-exponential T_1 decay, whereas bi-exponential $T_{1\rho}$ decay. These results indicate that nifedipine and PHPA are immiscible and that domains 5 to 50 nm in size are present in the solid dispersion. The nifedipine–PHPA solid dispersions (4 : 6 and 5 : 5) and the phenobarbital–PHPA solid dispersions (3 : 7) also exhibited bi-exponential $T_{1\rho}$ decay (data not shown). Figure 2 shows powder X-ray diffraction patterns of the nifedipine–PHPA and nifedipine–PVP solid dispersions. The observed halo pattern indicates that nifedipine in the PHPA dispersions is amorphous at the detection limit of powder X-ray diffractometry.

DSC data supported the contention that nifedipine and PHPA are immiscible. Figure 3 shows typical DSC traces for nifedipine–PHPA solid dispersions. The nifedipine–PHPA solid dispersion (3 : 7) showed glass transition at approximately 50 °C, corresponding to the T_g of amorphous nifedipine, and at approximately 75 °C, indicating that there are both an amorphous nifedipine phase and an amorphous nifedipine–PHPA phase in the solid dispersion. These DSC data indicate that amorphous nifedipine and PHPA are partially immiscible at this weight ratio. For the nifedipine–PHPA solid dispersion (5 : 5), T_g of the amorphous nifedipine–PHPA phase was not clearly observed because of the detection limit of DSC, suggesting that ^{1}H-NMR relaxation measurements can detect immiscibility of drugs and polymers more sensitively than DSC. DSC data suggest that the nifedipine–PHPA solid dispersion (3 : 7) consists of pure amorphous nifedipine phase and amorphous nifedipine–PHPA phase. NMR data may support this speculation. As shown in Fig. 1B, initial $T_{1\rho}$ decay of the solid dispersion was slower than that of the physical mixture or pure PHPA. This slow relaxation rate of the solid dispersion may indicate that the relaxation rate of PHPA protons was decreased by spin diffusion with nifedipine protons existing near PHPA molecules; in other words, nifedipine–PHPA phase is considered to exist in the solid dispersion. The effect of weight ratios on the $T_{1\rho}$ decay of nifedipine–PHPA solid dispersions needs to examine in order

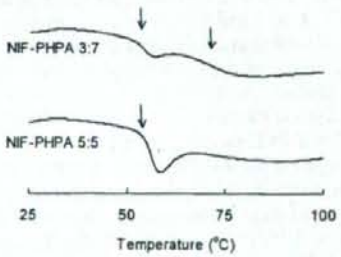

Fig. 3. DSC Traces for Nifedipine–PHPA Solid Dispersions
Arrows represent T_g

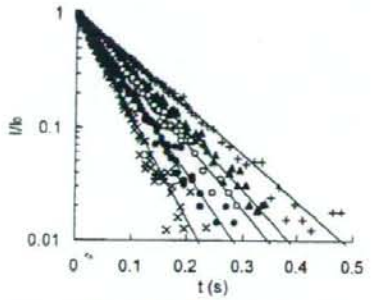

Fig. 4. $T_{1\rho}$ Decay Patterns for Nifedipine (+), PVP (×), and Nifedipine–PVP Solid Dispersions of 7 : 3 (▲), 5 : 5 (○), and 3 : 7 (●)

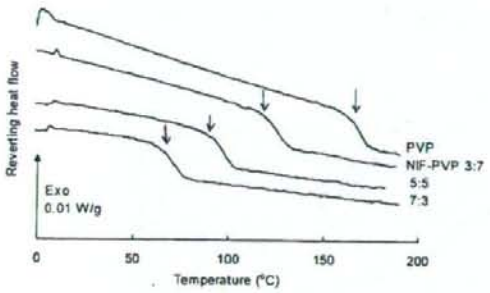

Fig. 5. DSC Traces for Nifedipine–PVP Solid Dispersions
Arrows represent T_g

to confirm the phase structure of the solid dispersion, since the molecular mobility of PHPA may different from that of pure PHPA.

In contrast to PHPA, PVP and nifedipine in the solid dispersions (3 : 7, 5 : 5 and 7 : 3) were considered to be miscible from $T_{1\rho}$ relaxation and DSC measurements. Figure 4 shows typical $T_{1\rho}$ decay of the solid dispersions. All the solid dispersions studied exhibited mono-exponential $T_{1\rho}$ decay, whereas physical mixtures of amorphous nifedipine and PVP (3 : 7, 5 : 5 and 7 : 3) exhibited bi-exponential decay (data not shown). Figure 5 shows DSC traces for the nifedipine–PVP solid dispersions. A single glass transition was observed for all of the solid dispersions studied. These data indicate that nifedipine and PVP are miscible at the detection limit of NMR and DSC.

For nifedipine–HPMC solid dispersions, the miscibility of nifedipine and HPMC could not be assessed from T_g measurements. As shown in Fig. 6, base line shift due to glass transition was not obvious for the nifedipine–HPMC solid dispersions (3 : 7 and 5 : 5). In contrast to DSC measurements, $T_{1\rho}$ relaxation measurements clearly indicated that nifedipine is miscible with HPMC in the solid dispersions. As shown in Fig. 7, all the nifedipine–HPMC solid dispersions studied showed mono-exponential $T_{1\rho}$ decay. In contrast to the solid dispersions, physical mixtures of amorphous nifedipine and HPMC (3 : 7, 5 : 5 and 7 : 3) exhibited bi-exponential decay (data not shown). These data indicate that NMR can detect miscibility of a drug and an excipient more sensitively than DSC.

Figure 8 shows the dissolution profile of nifedipine from

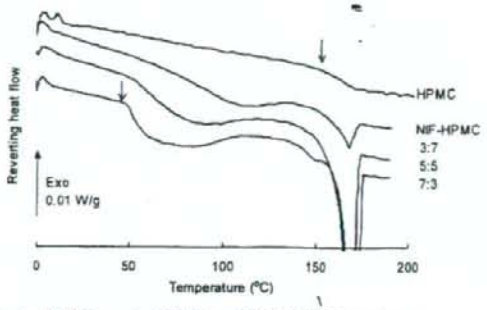

Fig. 6. DSC Traces for Nifedipine–HPMC Solid Dispersions
Arrows represent T_g

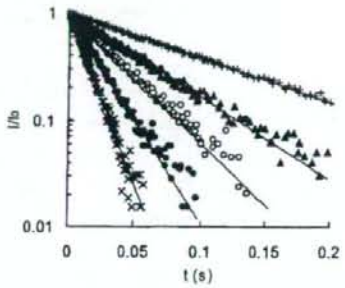

Fig. 7. $T_{1\rho}$ Decay Patterns for Nifedipine (+), HPMC (×), and Nifedipine–HPMC Solid Dispersions of 7 : 3 (▲), 5 : 5 (○), and 3 : 7 (●)

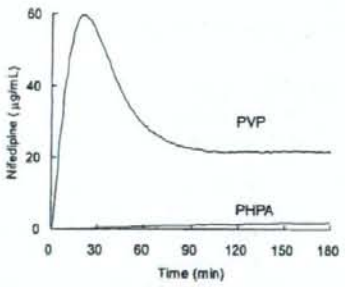

Fig. 8. Dissolution Profiles of Nifedipine from Solid Dispersions with PVP and PHPA

solid dispersions with PVP and PHPA. The nifedipine–PVP solid dispersion exhibited rapid dissolition of nifedipine with super-saturation. In contrast, only a minimal amount of nifedipine was dissolved from the nifedipine–PHPA solid dispersion.

In conclusion, ^{1}H- NMR spin–lattice relaxation measurements were found to be useful for assessing the miscibility of a drug and excipients in solid dispersions, especially, when T_g is not clearly detected by DSC. The lower miscibility of PHPA than that of PVP and HPMC with hydrophobic drugs is considered due to the more hydrophilic nature of PHPA.

Acknowledgements A part of this work was supported by a Grant-in-aid for Research on Publicly Essential Drugs and Medical Devices from The Japan Health Sciences Foundation.

References

1) Forster A., Hempenstall J., Tucker I., Rades T., *Int. J. Pharm.*, **226**, 147—161 (2001).
2) Lu Q., Zografi G., *Pharm. Res.*, **15**, 1202—1206 (1998).
3) Khougaz K., Clas S. D., *J. Pharm. Sci.*, **89**, 1325—1334 (2000).
4) Tong P., Zografi G., *J. Pharm. Sci.*, **90**, 1991—2004 (2001).
5) Vasanthavada M., Tong W. Q., Joshi Y., Kislalioglu M. S., *Pharm. Res.*, **21**, 1598—1606 (2004).
6) Shmeis R. A., Wang Z., Krill S. L., *Pharm. Res.*, **21**, 2025—2030 (2004).
7) Kaplan D. S., *J. Appl. Polym. Sci.*, **20**, 2615—2629 (1976).
8) Crowly K. J., Zografi G., *J. Pharm. Sci.*, **91**, 2150—2165 (2002).
9) Marsac P. J., Shamblin S. L., Taylor L. S., *Pharm. Res.*, **23**, 2417—2426 (2006).
10) Cheung M. K., *Polymer*, **41**, 1469—1474 (2000).
11) Asano A., Takegoshi K., "Solid State NMR of Polymers," Chap. 10, ed. by Ando I., Asakura T., Elsevier, Amsterdam, 1998, pp. 351—414.
12) Giammona G., Carlisi B., Piazzo S., *J. Polym. Sci. Polym. Chem. Ed.*, **25**, 2813 – 2818 (1987).
13) Kato Y., Watanabe F., *Yakugaku Zasshi*, **98**, 639—648 (1978).
14) Aso Y., Yoshioka S., Kojima S., *J. Pharm. Sci.*, **89**, 408—416 (2000).

Wide-Ranging Molecular Mobilities of Water in Active Pharmaceutical Ingredient (API) Hydrates as Determined by NMR Relaxation Times

SUMIE YOSHIOKA, YUKIO ASO, TSUTOMU OSAKO, TORU KAWANISHI

National Institute of Health Sciences, 1-18-1 Kamiyoga, Setagaya-ku, Tokyo 158-8501, Japan

Received 10 October 2007; revised 27 November 2007; accepted 28 November 2007

Published online 6 February 2008 in Wiley InterScience (www.interscience.wiley.com). DOI 10.1002/jps.21294

ABSTRACT: In order to examine the possibility of determining the molecular mobility of hydration water in active pharmaceutical ingredient (API) hydrates by NMR relaxation measurement, spin–spin relaxation and spin–lattice relaxation were measured for the 11 API hydrates listed in the Japanese Pharmacopeia using pulsed ^{1}H-NMR. For hydration water that has relatively high mobility and shows Lorentzian decay, molecular mobility as determined by spin–spin relaxation time (T_2) was correlated with ease of evaporation under both nonisothermal and isothermal conditions, as determined by DSC and water vapor sorption isotherm analysis, respectively. Thus, T_2 may be considered a useful parameter which indicates the molecular mobility of hydration water. In contrast, for hydration water that has low mobility and shows Gaussian decay, T_2 was found not to correlate with ease of evaporation under nonisothermal conditions, which suggests that in this case, the molecular mobility of hydration water was too low to be determined by T_2. A wide range of water mobilities was found among API hydrates, from low mobility that could not be evaluated by NMR relaxation time, such as that of the water molecules in pipemidic acid hydrate, to high mobility that could be evaluated by this method, such as that of the water molecules in ceftazidime hydrate.

 J Pharm Sci 97:4258–4268, 2008

Keywords: NMR relaxation time; dynamics; hydrate; DSC; water vapor sorption isotherm

INTRODUCTION

Correlations between chemical stability and molecular mobility have been demonstrated for various amorphous pharmaceuticals in the solid state.[1] Furthermore, the chemical stability of active pharmaceutical ingredient (API) hydrates is suggested to be correlated with the molecular mobility of water of hydration present in the crystalline structure.[2,3]

Water molecules in API hydrates exhibit a variety of physical states,[4,5] suggesting a range of molecular mobilities; water molecules incorporated into rigid crystalline structures may have low molecular mobility, whereas less rigid structures contain water molecules with greater mobility. Hydration water plays an important role in determining the physical characteristics—such as solubility[6] and flowability—of the API hydrate. Therefore, an understanding of the physical properties of hydration water, such as molecular mobility, is critical in the formulation of API hydrates.

The molecular mobility of water in solids may be determined by various methods, such as dielectric relaxation spectroscopy[7] and FT-Raman

Correspondence to: Sumie Yoshioka (Telephone: 81-3-3700-8547; Fax: 81-3-3707-6950; E-mail: yoshioka@nihs.go.jp)

Journal of Pharmaceutical Sciences, Vol. 97, 4258–4268 (2008)

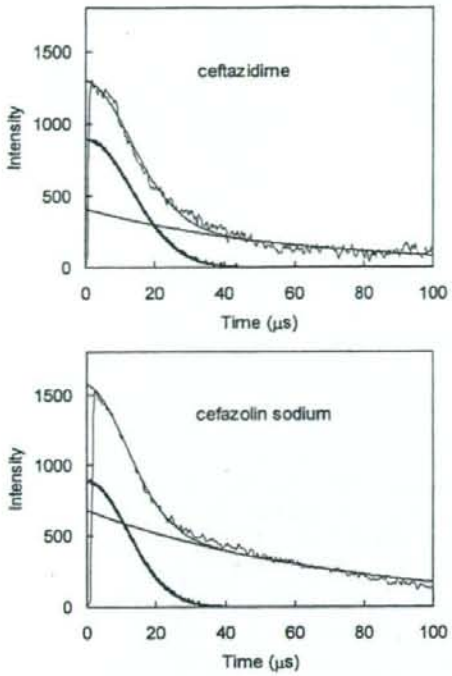

Figure 1. Free induction decay for ceftazidime and cefazolin sodium hydrates.

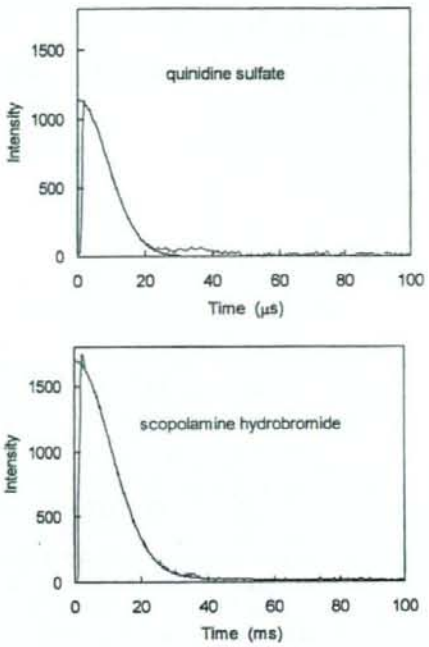

Figure 2. Free induction decay for quinidine sulfate and scopolamine hydrobromide hydrates.

spectroscopy.[8] NMR is also utilized to determine the molecular mobility of water in the solid state,[9] and to examine the various mechanisms by which solids interact with water.[10,11] However, there have been few studies in which the molecular mobility of water in API hydrates was determined using NMR. This may be because ^{1}H-NMR, even high resolution ^{1}H-NMR, cannot separate the peaks of the water protons from those of the protons in other components, which prevents specific determination of water mobility. Although the preparation of API hydrate samples using ^{17}O-labeled water allows to specifically determine the mobility of the water molecules by ^{17}O-NMR, unaffected by the other components, this approach requires high cost and much labor.

Table 1. Water Content of API Hydrates

API Hydrate	Number of H_2O per Molecule Specified in JP	Number of H_2O per Molecule Determined by KF	Spin–Spin Relaxation of H_2O
Cefazolin sodium	5	4.67	Lorentzian
Ceftazidime	5	5.04	Lorentzian
Amoxicillin	3	2.94	Lorentzian
Ampicillin	3	2.96	Lorentzian
Berberine Chloride	Not specified	2.67	Gaussian
Quinine hydrochloride	2	1.31	Gaussian
Scopolamine hydrobromide	3	2.32	Gaussian
Saccharin sodium	2	1.15	Gaussian
Pipemidic acid	3	2.9	Gaussian
Sulpyrine	1	0.98	Gaussian
Quinidine sulfate	2	1.95	Gaussian